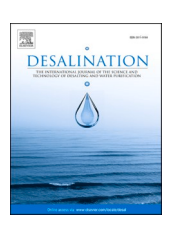
ELSEVIER

Contents lists available at ScienceDirect

Desalination

journal homepage: www.elsevier.com/locate/desal





Desalination metamodels and a framework for cross-comparative performance simulations

Sebastian A. Romo*, Nicholas Mattise, Jelena Srebric

Department of Mechanical Engineering, University of Maryland, College Park, MD 20742, USA

HIGHLIGHTS

- Study metamodels include six desalination processes classified as thermal or molecular.
- Reduced-order metamodels can accurately reproduce desalination transport processes.
- The largest error when comparing metamodel results to published data is 9%.
- The study grouped and prioritized inputs and outputs for all metamodel data.
- These data structures enabled a cross-comparative framework of desalination processes.

ARTICLE INFO

Keywords: Cross-comparison Multi-Effect Distillation Reverse Osmosis Energy consumption Desalination modeling

ABSTRACT

There is an opportunity to save energy and reduce operational expenses when choosing a suitable desalination method aided by computational modeling. Existing models are not conducive to generalized comparisons between different desalination methods. Therefore, this study developed metamodels for six desalination methods, grouped them into thermal and molecular transport families, and validated their predictive performance within 9% difference from published data. This validated framework allowed comparisons of desalination methods at their prescribed ranges of operational conditions that they were designed for. These conditions specify feed salinity ranges of 1.6 to 2.4 g/kg for Capacitive Deionization and Reverse Osmosis (RO), 2.8 to 4.2 g/kg for Electrodialysis, 28 to 42 g/kg for Thermovapor Compression and Humidification-Dehumidification, and 37 to 55 g/kg for Multi-Effect Distillation (MED). Despite different operational conditions, all models exhibit non-linear, positive correlation between energy consumption and system size in response to feed salinity and production rate. The framework is also employed in a cross-comparative analysis between MED and RO whose results suggest that energy intensity for MED is an order of magnitude greater than RO for the same operational conditions, but actual operational costs are comparable. Overall, the framework is ready for deployment in case studies of actual desalination plants.

1. Introduction

Different desalination processes have been developed over the years to increase efficiency, reduce equipment maintenance, or target water with higher salt contents. There are more than ten different desalination methods and countless system variations within each method, each one particularly useful for specific feed water characteristics and production requirements. While there have been many efforts to model each process individually for optimization, cross-comparison of desalination technologies remains a major challenge due several factors including: the lack of standardization in modeling algorithms, difficulties in

reproducing modeling approaches because of undisclosed parameters or equations, and models learned with data from a specific system but that cannot be generalized to broader operational ranges.

The starting point towards overcoming this challenge is to correctly implement the models of the most common desalination technologies under a common framework with matching computational structures and parameters. The literature presents volumes of case studies and technological developments with scattered models. Furthermore, most studies do not disclose all required variables or correlations involved in the simulation algorithm and make the model replication and validation particularly challenging. Although some cases perform comparison of

E-mail addresses: sromo1@umd.edu (S.A. Romo), jsrebric@umd.edu (J. Srebric).

^{*} Corresponding author.

two desalination technologies side-by-side and find equivalent metrics, there is still no standard framework to equalize the input domains of multiple desalination processes simultaneously.

The literature reflects a lack of cohesion in modeling purposes among the different desalination studies. There are commonly accepted desalination models that are predictive in nature, but there is no common algorithm structure that allows for cross-comparison. The greatest challenge in achieving this lies in the lack of knowledge on the physics behind some sub-processes that take place in different desalination systems. Most modeling approaches resort to regression and empirical correlations that are valid for the specific operational conditions and particular system that data is measured from. This is complicated by the lack of disclosure of modeling equations, important parameters, or correlation coefficients in published literature which challenges collaboration among the desalination community. Further research is required into developing such mechanistic equations to expand the predictive capabilities of desalination models. On the other hand, the literature presents many models with different simulation objectives and different input-output structures, which cannot be executed in parallel and therefore do not allow direct comparisons of the results. It is important to organize model algorithms to follow similar input-outputs structures to impose similar constraints to the system and enable meaningful cross-comparison of different desalination technologies.

Few research efforts have focused on comparison between different desalination technologies, and the extent to which such crosscomparison methodologies are implemented present great differences. The majority of studies enumerate and review the general operational ranges such as the feed concentration and product water flow rate that different technologies are able to process [1-6]. However, the implementation of such findings is limited to general statistical models that might not be representative of the actual system performance at the required operational conditions [7]. Later research efforts recognized the importance in evaluating energy consumption of desalination technologies and consider the high-level breakdown in heat and electricity requirements [8]. Comparing energy consumption is an initial step into finding universal parameters among desalination technologies that can provide meaningful insights. Finally, a few more recent studies simulate energy consumption from a thermodynamic law analysis [9,10]. In general, cross-comparison studies in the literature are limited to pairwise comparisons between desalination methods focusing on energy and cost at discrete operation points [11–15]. A more robust comparison of different desalination systems can be conducted through an exergy analysis, which captures the effects of different operation conditions [16]. Although correct from a theoretical standpoint, reducing system operation to a single operation term is often not enough for practical decision making. Pairwise comparison approaches are valuable and can be an excellent complement to a holistic comparison that considers all involved parameters such as flow rates, concentrations, system sizes and performance metrics. To the best of our knowledge, a modeling framework that enables a holistic and direct cross-comparison between different desalination methods has not yet been proposed. The first step towards implementing such framework is to classify the different desalination models and establish hierarchical input-output structures that dictates the extent to which different desalination processes can be cross-compared.

The present study proposes a framework for cross-comparison between desalination technologies centered on a standard hierarchical structure for model inputs and outputs, consistent model computational structures, and standardized sets of thermophysical property correlations that include temperature, pressure, and salinity dependence. We first organize the knowledge of desalination modeling to develop metamodels for six different desalination processes including Thermovapor Compression (TVC), Multi-Effect Distillation (MED), Humidification-Dehumidification (HDH), Reverse Osmosis (RO), Electrodialysis (ED) and Capacitive Deionization (CDI). Then, we deploy the proposed framework in a generalized comparison between the aforementioned

desalination methods whose similar energy consumption patterns and responses to product flow rate and feed salt concentration suggests that apparent differences between desalination processes are superficial and that they actually share compatible transport processes. Finally, we apply our framework in a full cross-comparative analysis between MED and RO which are currently the most relevant desalination methods, and identify the benchmarks that developing technologies must cater to in the desalination market.

2. Methodology

The first step in developing a cross-comparison enabling simulation framework is to correctly implement the models available in the literature. The systematized process of literature review and implementation is shown in Fig. 1. We used scientific publication databases like ScienceDirect and Google Scholar to search for the desalination method name plus the key words "modeling" and "desalination." We considered peerreviewed research articles, book chapters, and theses for this review.

Most published models unfortunately do not disclose all the required parameters or equations, and many can only simulate a single specific set of operational conditions. To resolve this, we develop metamodels that supplement a representative model structure with sub-component models from different studies. The metamodel development process, therefore, is iterative in nature and dictates the direction of the literature review. The most representative model is the literature model where the complete modeling equations are disclosed, and reference values are provided. Additionally, the selection criteria for the most representative model prioritizes reduced-order models, which have low algorithmic complexity and computational intensity requirements but are still capable of capturing specific differences between operation conditions. The most representative model serves as a guide for the main code structure and provides numerical inputs and outputs for validation. Most models available in the literature unfortunately do not disclose the complete set of variables or equations to close the water/energy/product balance equations needed for implementation in an analytical framework. In the cases where equations, coefficients, or parameters are missing, we conducted further literature review from other references found in the initial search or a new targeted search for the specific unknowns. This iterative process continued until all the initial number of references was reviewed and the metamodel was completed. The resulting metamodel is validated with the values of the most representative model targeting a maximum allowable difference of 10% in the inputs and outputs associated to flow rate, concentration, energy intensity, and system sizing. If the target was not met, we returned to reviewing literature in search of more detailed sub-models.

After successful validation, we standardized the computational

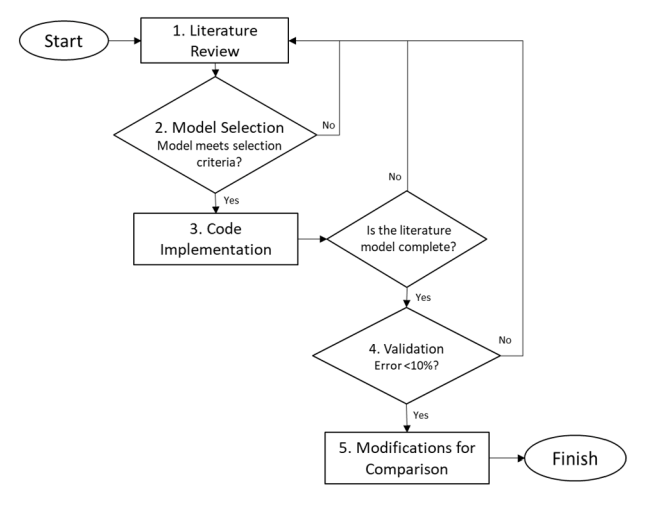


Fig. 1. Meta-study research and implementation process.

 Table 1

 Number of curated references used for each developed desalination model.

| Desalination process | Ref. No. | Selected lit. model |
|---------------------------------------|----------|---------------------|
| Thermovapor Compression (TVC) | 34 | [24] |
| Multi-Effect Distillation (MED) | 28 | [25] |
| Humidification-Dehumidification (HDH) | 19 | [26] |
| Reverse Osmosis (RO) | 50 | [27] |
| Electrodialysis (EDS) | 40 | [28] |
| Capacitive Deionization (CDI) | 64 | [29] |
| Total | 235 | |

structure and matched the hierarchical set of inputs and outputs proposed in this section to enable cross-comparison among different models. In this step, the thermophysical properties of the working fluids are also standardized using correlations that cover the largest validity ranges and consider temperatures, pressures, and salt concentrations when appropriate [17–23]. The resulting metamodel is an improved version of the original literature model re-engineered for the specific purpose of design and cross-comparison between different technologies. Finally, we use the incomplete sets of numerical inputs and outputs found through the literature review process, when available, to test the metamodel with a wider range of inputs. The unknown parameters are supplemented by other studies that disclose them and have the most similar operation conditions. This testing does not impose a maximum allowable difference but rather shows how generalizable the resulting metamodel is.

Table 1 shows the total number of studies reviewed through the development of each metamodel presented in this paper and the selected literature models that guided validation.

3. Results

We present the results of our research in two parts. The first part considers metamodel development for each desalination method including Thermovapor Compression, Multi-Effect Distillation, Humidification-Dehumidification, Reverse Osmosis, Electrodialysis and Capacitive Deionization. All equations necessary to model the corresponding system are disclosed within each section. The relevant equations of the metamodels provided within each description are implemented in an open-source, cloud-based application [30].

The second part elucidates on the cross-comparison enabling simulation framework that controls the execution of the proposed metamodels. The complete list of inputs and expected outputs for each model under the proposed simulation framework are listed in Table 9 at the end of the section. The framework is then deployed on all developed metamodels to support that almost identical patterns can be observed in the energy intensity response to changes in product flow rates and feed salinity. Finally, a full cross-comparison between the most commercially

competitive processes, Multi-Effect Distillation and Reverse Osmosis, suggests that the cost of energy process benefits of Multi-Effect Distillation must justify its considerably larger energy intensity.

3.1. Metamodels for desalination processes

All metamodels integrate submodels and thermophysical property functions from a variety of studies to expand the validity of the model while maintaining computational simplicity. These metamodels are classified according to the separation process featured in each method, which is also aligned with the type of thermophysical properties involved in the calculations. For instance, the thermal family involves properties such as enthalpies and latent heat, while the molecular transport family involves properties like permeability and conductivity. Table 2 summarizes the high-level simulation parameters validated within 9% with the relevant parameters from the most representative literature model. In the case of intermediate parameters for MED and HDH, there is a maximum difference of 15% with the flashed distillate flow rate, and 64% difference with the cooling water flow rate. For MED, the difference is caused because the literature model assumes constant thermophysical properties while all our metamodels incorporate temperature, pressure, and salinity dependence [17–23]. The discrepancy in HDH, on the other hand, is not clearly labeled in the published study and is likely a simple typographical error. It must be noted however, these parameters have minimum impact in energy consumption calculations. All other parameters in all the developed models show excellent agreement with literature data overall. The complete validation tables with the selected model and additional studies are found in the paper

The successful validation of the metamodels with their corresponding representative model from the literature demonstrates they satisfactorily meet their intended purpose. However, the parameters shown in Table 2 represent only one possible operation point of each desalination system. Therefore, further validation is conducted with additional studies that show different operation conditions, including product flow rates and feed water salinities. The reader is encouraged to refer to the complete validation tables which list the complete sets of inputs, outputs, and relevant intermediate parameters in the Appendix. The unknown input fields in these cases are supplemented with values from other studies. Priority is given to the studies with most similar operation conditions for the cases where multiple options to supplement an unknown input exist. It is expected that the additional validation points have a larger percent difference from the metamodel because the correlations, modeling algorithm and unknown values would differ slightly. Nevertheless, the metamodel results show great agreement with all independent studies.

 Table 2

 Validation summary of the metamodels with their corresponding most representative model literature from the literature (Full table in the Appendix).

| • | | 0 1 | | | ` | * |
|---|-------------|------------|------------|-------------------|-------------|--------------|
| | TVC | MED | HDH | RO | EDS | CDI |
| Selected lit. model | [24] | [25] | [26] | [27] | [28] | [29] |
| Family | Thermal | | | Molecular transpo | ort | |
| Product flow rate, M_d (kg/s) | 0.5787 [0%] | 137.9 [0%] | 1.156 [0%] | 2.087 [0%] | 4.051 [0%] | 6.138e-5 [-] |
| Intake salinity, C_f (g/kg) | 35 [0%] | 46 [0%] | 35 [-] | 2 [0%] | 3.5 [0%] | 2 [0%] |
| Intake temp. T_{in} (°C) | 25 [0%] | 28 [0%] | 25 [0%] | 20 [0%] | 20 [-] | 25 [-] |
| Feed water flow rate, M_f (kg/s) | 1.360 [2%] | 366.9 [4%] | 16.87 [0%] | 3.472 [-] | 5.401 [-] | 6.138e-5 [-] |
| Brine flow rate, M_b (kg/s) | 0.7811 [-] | 234.4 [4%] | 15.48 [1%] | 1.383 [-] | 1.360 [-] | 6.138e-5 [-] |
| Product water salinity, C_p (g/kg) | 0 [-] | 0 [0%] | 0 [0%] | 0.023 [-] | 0.35 [0%] | 0.70 [-] |
| Brine salinity, C_b (g/kg) | 60.9 [2%] | 72 [0%] | 38.2 [-] | 4.99 [0%] | 13.0 [3%] | 2.54 [-] |
| Specific energy, E _{des} (kWh/m ³) | 239.9 [-] | 66.37 [-] | 486.5 [-] | 0.9099 [-] | 0.3688 [9%] | 0.5594 [8%] |
| | | | | | | |

[%]: Percent difference. This value is not calculated for the parameters that are not provided explicitly in the literature model.

3.1.1. Thermovapor Compression

A Thermovapor Compression (TVC) desalination system has three main components: a condenser, one or more evaporators, and a thermoejector. For the interests of this study, we consider only a single evaporator system although there are models in the literature that include multiple cascading evaporators [31,32]. As shown in Fig. 2, TVC desalination is driven by a motive steam flow rate (M_p) which mixes and is ejected in the thermocompressor with an entrained water vapor flow (M_e) , extracted from the vapor stream produced in the evaporator side. The resulting mixed steam stream that supplies necessary heat in the evaporator to separate feed water flow rate (M_f) into water vapor and brine (M_b) flows by overcoming the boiling point elevation caused by salt presence in the fluid [33]. The proposed TVC metamodel does not consider circulation pump energy consumption as it is insignificant when compared to the total heat input to the system. Table 3 describes the relevant TVC metamodel equations which are solved in a forward sequential algorithm and implemented through the proposed simulation framework at the end of the Results section.

The steam ejector is a key component of TVC with contrasting modeling approaches. Several desalination steam ejector models are available in the literature, each one with different assumptions and modeling detail. While recent studies present physical models with great validity [34,35], they require additional inputs that are not available in published TVC models. There are other high-level empirical models [36,37], based on graphical operational curves [38], that are suitable for the present application but have narrow operational ranges. We found the most appropriate model for this study to consist of empirical correlations that expand the validity range of the aforementioned operational curves while maintaining a relevant level of abstraction [39].

The ejected steam from the thermocompressor supplies heat in one side of the evaporator to separate the saline feed water into a water vapor and brine streams in the other side. Part of this generated water vapor is eventually recirculated in the thermoejector, and the remaining is condensed into the product water in the condenser. Heat transfer coefficients (HTC's) are modeled trough empirical correlations consistently used throughout the literature. El-Dessouky et al. [22] compiled evaporator and condenser HTC's with different fouling or flow characteristics. We employ the overall temperature-dependent HTC correlations that combine such variations and can be found across several desalination models with slight variations in significant digits [24,40–42].

The water vapor stream produced in the evaporator may have entrained saline water droplets produced from the impact of the saline water jets onto the evaporator tubes. A wire-mesh demister is often used to capture such saline droplets in the flow and induces a pressure drop in the vapor flow. The demister pressure drop is modeled through empirical correlations that consider demister properties such as pad density, thickness or wire diameter, and the vapor velocity through the demister [22,43–45]. We found that these correlation coefficients were often modified without explanation; therefore, we opted to use the correlations from a study that provides a reference pressure drop value so that we could verify coefficients and units [24].

These different approaches to modeling TVC systems can be due to different research objectives in each study. For instance, some of the early models focus on parametric analysis of a generic TVC system [37,45], while the more recent models propose a parametric study with updated thermoejector modeling strategies [24]. The models used in more recent studies focused on optimization strategies for real-life desalination plant models that feature more than a single evaporator [32,36]. Finally a different study highlighted another use of a TVC model in analyzing the performance of the system in response to feed water seasonality changes [31].

3.1.2. Multi-Effect Distillation

Multi-Effect Distillation (MED), like TVC, is based on the evaporation of water from a feed saline stream, however, this process features several evaporators denominated "effects" which are connected in series. Motive steam flows into the first effect only in one side of the heat exchanger and the other effects intake the water vapor generated in the prior effect (*i.e.* steam generated in the first effect supplies heat to the second effect, the latter into the third effect, and so on through all the effects). Electricity consumption in pumps is neglected in the proposed MED metamodel as it is insignificant in comparison to the heat input to the system. Table 4 details the relevant MED metamodel equations which are solved in a forward sequential algorithm that iterates through each effect within the system.

There are three configurations of MED that differentiate in how the feed saline water flows with respect to the generated vapor in each effect. Forward feed is the most extensively modeled configuration [22,40,46], in which all the saline feed is directed to the first effect, and the brine generated in each effect is then directed as feed into the subsequent effect. This configuration, however, is not practical in the

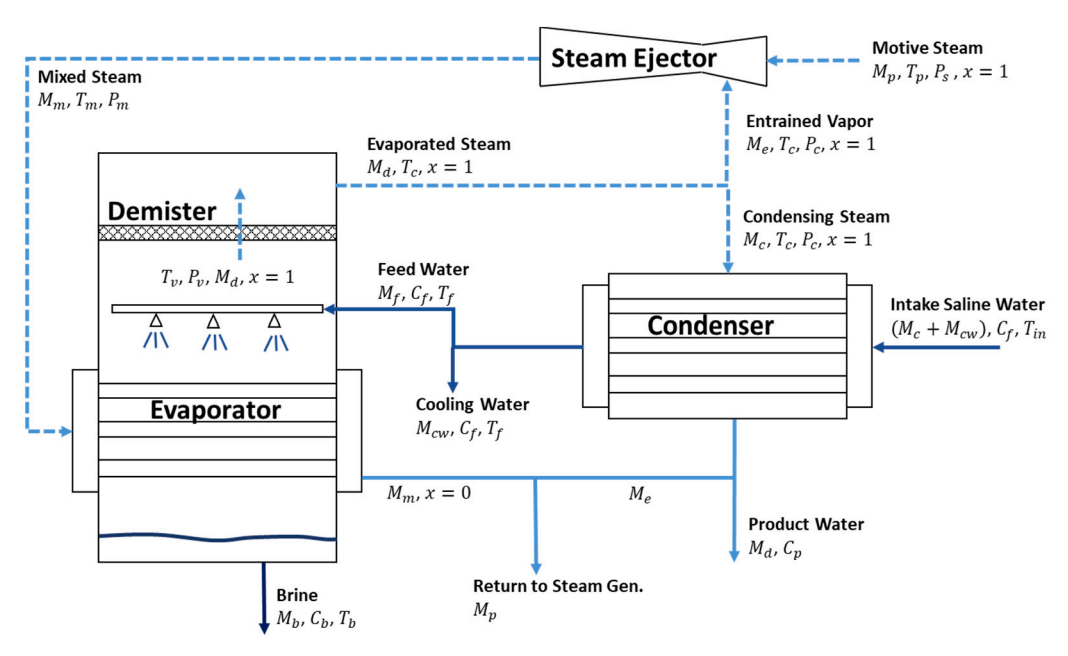


Fig. 2. TVC process schematic.

Table 3 TVC metamodel key equations.

| Component | Equation | | Variable | s | Ref. |
|----------------|--|-----|-----------------|--|--------|
| Condenser | $M_c\lambda_c=(M_f+M_{cw})c_p(T_f-T_{in})$ | (1) | M_c | Vapor flow rate | [24] |
| | | | λ_c | Latent heat | |
| | | | M_f | Feed water flow rate | |
| | | | M_{cw} | Cooling water flow rate | |
| | | | c_p | Specific heat | |
| | | | $\dot{T_f}$ | Feed water temperature | |
| | | | T_{in} | Intake water temperature | |
| Evaporator | $M_m(h_m-h_{x=0})=M_fc_p(T_b-T_f)+M_d\lambda_d$ | (2) | M_m | Mixed steam flow rate | [24] |
| • | , , , , , , , , , , , , , , , , , , , | | h_m | Mixed steam enthalpy | |
| | | | $h_{x=0}$ | Mixed steam saturation enthalpy | |
| | | | T_b | Brine temperature | |
| | | | M_d | Vapor product | |
| | | | λ_d | Latent heat | |
| Demister | $\Delta P_{de} = 9.583 \times 10^{-5} \rho_{de}^{1.597} V_{de}^{0.7197} L_{de}^{1.388}$ | (3) | ΔP_{de} | Pressure drop | [24,4 |
| | , | | Pde | Demister packing density | |
| | | | V_{de} | Vapor velocity in demister | |
| | | | L_{de} | Demister thickness | |
| Thermoejector | [1] | (4) | A | Regression constants | [38,39 |
| , | | | В | Regression constants | |
| | $M_r = \sum_{n=0}^3 \left(A_n C_r^n + rac{B_n}{E_r^n} ight) + rac{C_r}{E_r} C \cdot egin{bmatrix} 1 \ C_r \ 1/E_r \end{bmatrix}$ | | С | Regression constants | |
| | If $E_r \geq 100, 100 \geq E_r \geq 10$ | | | | |
| | [1] | (5) | C_r | Compression ratio | |
| | $a = \begin{pmatrix} B_{-} \end{pmatrix} \begin{pmatrix} C_{-} & 1 & 1 \\ 1 & 1 & 1 \end{pmatrix}$ | | E_r | Expansion ratio | |
| | $M_r = \sum_{n=0}^3 \left(A_n ln(C_r)^n + \frac{B_n}{E_r^n} \right) + \frac{C_r}{E_r} C \cdot \begin{bmatrix} 1 \\ ln(C_r) \end{bmatrix}_{1/E_r}$ | | M_r | Mass ratio | |
| | If $10 \geq E_r \geq 2$ | | | | |
| Evaporator HTC | $U_e = 1969.5 + 12.057T_b - 8.5989 \times 10^{-2}T_b^2 + 2.5651 \times \times 10^{-4}T_b^3$ | (6) | U_e | Evaporator heat transfer coefficient | [24] |
| Condenser HTC | $U_c = 1719.4 + 3.2063T_c + 1.5971 \times 10^{-2}T_c^2 - 1.9918 \times 10^{-4}T_c^3$ | (7) | U_c | Condenser heat transfer coefficient | [24,45 |
| | | | T_c | Steam temperature at the condenser inlet | |

Table 4
MED metamodel key equations.

| Component | Equation | | Variables | | Ref. |
|----------------|--|------|--------------------|--|------------|
| Condenser | $(M_{cw}+M_f)c_p(T_f-T_{in})=M_{d,\ end}\lambda_{d,\ end}$ | (8) | $M_{d, end}$ | Vapor flow rate from last effect | [25,64] |
| | | | $\lambda_{d, end}$ | Latent heat | |
| | | | M_f | Feed water flow rate | |
| | | | M_{cw} | Cooling water flow rate | |
| | | | c_p | Specific heat | |
| | | | T_f | Feed water temperature | |
| | | | T_{in} | Intake water temperature | |
| Evaporator | $M_p \lambda_p = M_{f, i} c_{p, i} (T_{b, i} - T_f) + D_{b, i} \lambda_{b, i}$ | (9) | M_p | Steam flow rate | [25,64] |
| | | | λ_p | Steam latent heat | |
| | | | $M_{f, i}$ | Feed water flow rate at ith effect | |
| | | | $c_{p, i}$ | Specific heat | |
| | | | $T_{b, i}$ | Brine temperature in ith effect | |
| | | | T_f | Feed water temperature | |
| | | | $D_{b,\ i}$ | Distillate produced by boiling in the ith effect | |
| | | | $\lambda_{b, i}$ | Latent heat | |
| Demister | $\Delta P_{de} = 3.88178 \rho_{de}^{0.375798} V_{\nu}^{0.81317} L_p d_p^{-1.56114147}$ | (10) | ΔP_{de} | Pressure drop | [22,44] |
| | | | ρ_{de} | Demister packing density | |
| | | | V_{de} | Vapor velocity | |
| | | | L_p | Packing length | |
| | | | d_p | Packing diameter | |
| Evaporator HTC | $U_e = 1969.5 + 12.057T_s - 8.5989 \times 10^{-2}T_s^2 + 2.5651 \times 10^{-4}T_s^3$ | (11) | T_s | Saturation temperature of steam | [24,65] |
| | | | U_e | Evaporator heat transfer coefficient | |
| Condenser HTC | $U_c = 1719.4 + 3.2063T_c + 1.5971 \times 10^{-2}T_c^2 - 1.9918 \times 10^{-4}T_c^3$ | (12) | T_c | Vapor temperature at condenser inlet | [24,45,65] |
| | | | U_c | Condenser heat transfer coefficient | |

desalination industry because it features the most complex layout [22]. In the backward feed configuration, the saline feed is directed to the last effect, and the generated brine is passed backwards from each effect until the first effect is reached. This implementation has a high risk of scaling because the highest salinity of the feed stream occurs in the first effect, which also has the highest temperature [47,48]. In addition, BF systems require higher pumping power as the saline feed must be pumped from lower to higher pressure effects [22,49]. Parallel feed is the most reliable MED configuration for desalination because it allows

the highest distillate production per motive steam consumed and generally requires less heat exchanger area [49]. In this configuration the feed water stream is split and directed into all effects simultaneously. We model a parallel feed MED system with no thermoejector for the purposes of this study, as shown in Fig. 3.

Published MED models present different assumptions regarding fluid thermophysical properties. For instance, some models assume constant properties such as or average boiling point elevation (BPE), specific heat capacity, and latent heat [25]. Others use a combination of constant

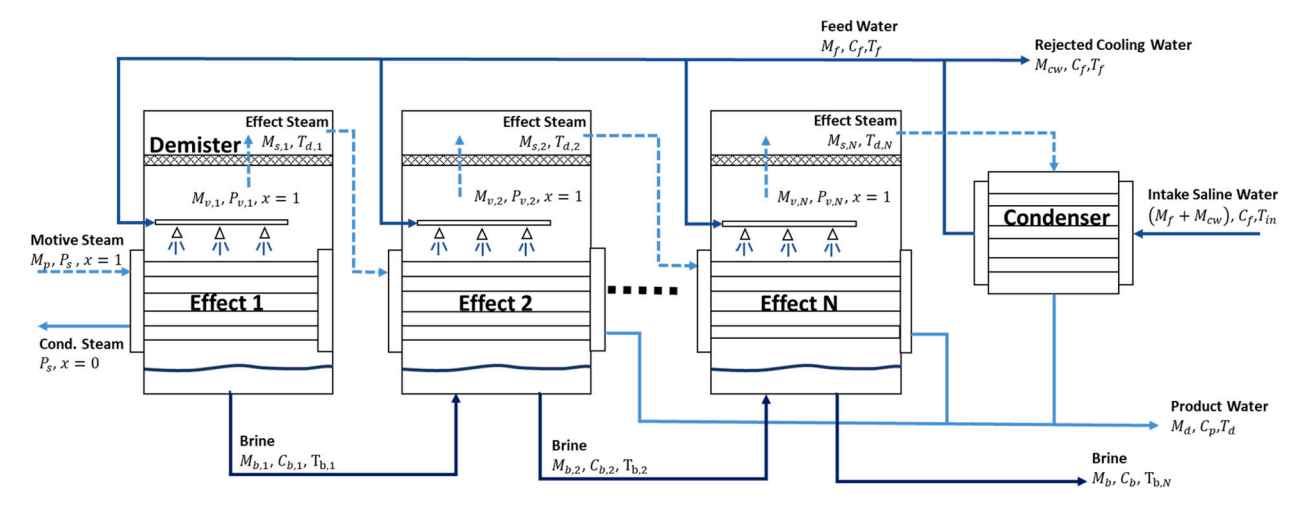


Fig. 3. MED process schematic.

properties for the water vapor or saline streams and temperature dependent correlations for the water stream [50,51]. Finally, there are models that feature temperature-based correlations for water and water vapor and include salinity effects for seawater thermophysical properties [40]. Like all metamodels presented in this paper, the MED metamodel features thermophysical function libraries that include temperature, pressure, and salinity dependence. Most saline and pure water properties are calculated using the Thermophysical Properties of Seawater library [17,18], and two-phase vapor-steam properties are calculated using the XSteam library [21]. Both XSteam and the Seawater libraries, however, could be used interchangeably at zero salinity. MED effects generally have a decreasing pressure profile which can promote vapor flashing as brine water is transferred from a previous effect at higher temperature into the subsequent effect. [25,52]. In some instances, MED units include flashing boxes to redirect steam for feed preheating or to add into the steam stream that is directed into the next effect [40,51,53]. It must be noted that flashing is not the main process through which vapor is generated, and therefore, some studies do neglect it [50]. Our metamodel implements flashing within each effect according to the saturation pressure that each effect maintains.

There are further differences between literature models regarding the modeling approach of each effect and the components within. There are models that assume constant heat transfer coefficients and fixed heat exchanger areas [25] while other models assume equal areas only [40]. In these calculations several studies employ the same vapor temperature-dependent HTC correlations as the models, described in the previous TVC section [50,54]. Within the reviewed MED models, few consider small pressure drop caused by the demister within each effect [54–56]. Finally, some MED models consider feed preheaters, which are heat exchangers before one or more effects that use steam (in some cases from an external process) to heat the feed water stream before entering the effect [25,46,50]. The energy required in the preheaters is generally small compared to the energy involved in water distillation but is found in actual case study data [57,58]. Our metamodel incorporates temperature-dependent HTC correlations commonly found in thermal desalination models [24,40-42], and correlations for the demister pressure drop [44]. For simplification, we assume preheating does not factor into the system's energy intensity and overwrite the constant feed temperature with the target preheat temperature at the desired effect. Nevertheless, considering the energy for feed preheating in this case can account for an increase in energy intensity of up to 20%.

These different modeling approaches have been developed to analyze different aspects of MED desalination. Early models were used in parametric studies of generic systems [40,55]. In the following years, studies used MED models to conduct studies of real-life desalination plants [50,59,60] and parametric analysis of MED systems with

thermocompression [51,56,61]. The latest modeling studies focused on analyzing the performance of MED desalination coupled with power cycles [53,54,62], and exploring the integration with solar energy [52,63].

3.1.3. Humidification-Dehumidification

Humidification Dehumidification (HDH) desalination makes use of the capacity of dry air to absorb and release moisture through psychometric processes. An Open-Air Open-Water (OAOW) HDH system, shown in Fig. 4, contains three main components including the dehumidifier, which fulfills a similar role to the condenser in TVC and MED desalination, a heater, and a humidifier. Cool saline water flows into the dehumidifier and gets preheated as hot humid air condenses in the other side. The intake stream flow is regulated by rejecting some of the preheated water as cooling water, and the remaining flows into the heater. The feed saline water is heated using the energy released from saturated steam inside the heater. The hot saline water is then sprayed in the humidifier, where it mixes with dry intake air. In this component the air absorbs moisture and exits as hot humid air into the dehumidifier, and the remaining water is rejected as saline brine. In the dehumidifier, the moisture from the humid air is collected as product water and the remaining air is exhausted. Circulation pump and fan energy consumption are neglected like the other thermal desalination metamodels. Table 5 shows the relevant HDH metamodel equations which are solved in a forward sequential algorithm through each component in the system.

The OAOW HDH system can be modified by changing the stream in which the heater is located or by closing and recirculating either the air or water loop. In addition, there is an air-heated configuration where the intake air, as opposed to the feed saline water flows through the heater. Both water-heated and air-heated cycles have similar production rates and energy input requirements, nevertheless, the air-heated cycle needs a larger air flow rate compared to the water heated cycle, and thus requires a larger fan and dehumidifier than the water-heated system [66]. The air loop in the system can remain open if the intake air temperature and humidity are low enough to facilitate moisture absorption, if this is not viable, the exhaust air can be recirculated to replace the intake air. Fewer instances of closed-water loop systems are found in the literature; while Closed-Air Open-Water (CAOW) and Closed-Water Open-Air (CWOA) water-heated systems have similar production rates of desalted water per steam consumed, recirculating saline water within the system requires additional control mechanisms to prevent scale formation [67–69]. Therefore, we implement the OAOW configuration for our proposed HDH metamodel.

The HDH process deals with saline water and moist air streams whose thermodynamic properties present different assumptions in the

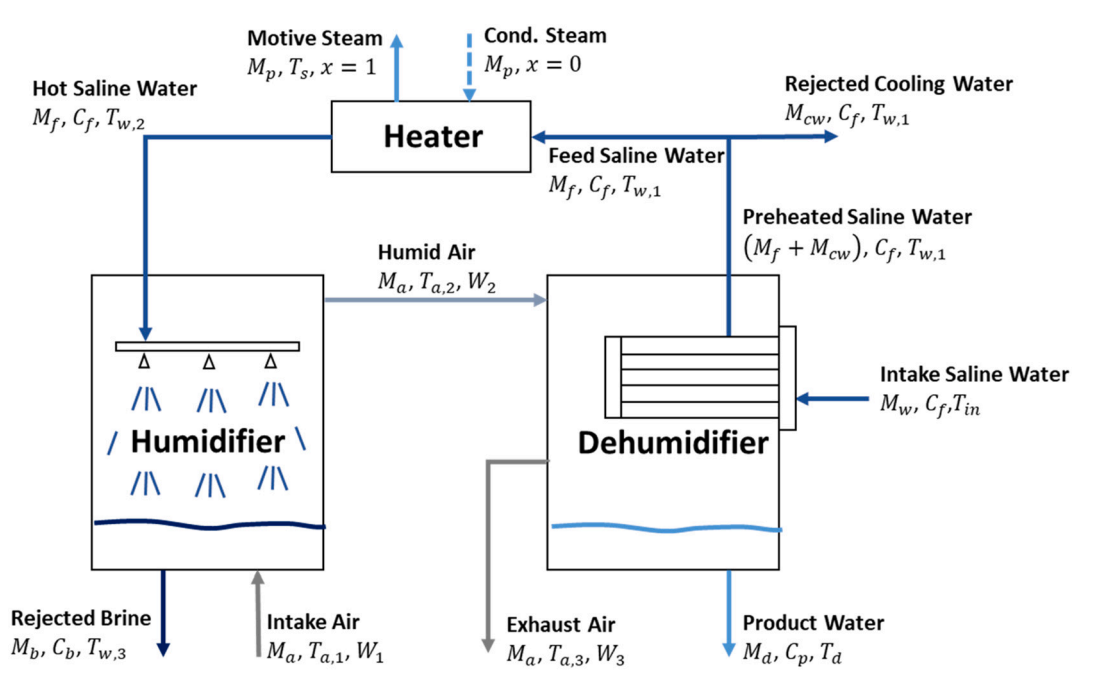


Fig. 4. HDH process schematic.

published studies. While all studies use common psychrometric property equations for moist air, they differ in saline water thermodynamic property calculations with increasing degrees of complexity. For instance, there are cases that employ correlations that do not consider the presence of salt in the fluid [70] and some that consider salt as the only independent variable [71]. The majority of desalination models employ either temperature and salinity dependent thermodynamic property correlations for saline water [26,72] or correlations that consider pressure effects in addition to temperature and salinity [66,73]. Like the other desalination processes, we incorporate thermophysical property functions that consider temperature, pressure and concentration for saline water [17,18], and moist air property functions with temperature, pressure and humidity dependence [23,74,75].

The literature presents different modeling approaches to the components of a HDH system, predominantly in the humidifier. The earlier HDH models use humidifier correlations that consider air and water flows and temperatures, and mass transfer coefficients [76]. The vast majority of studies use either standalone empirical correlations [70,77] or a combined approach between energy conservation assisted by numerical correlations [78,79]. And finally, one of the more recent studies employ iterative numerical methods for modeling the humidifier [66]. Similar differences are observed for modeling the heat transfer coefficients in the system including constant heat transfer coefficients [26] or the use of temperature-dependent empirical correlations [72]. We implement humidifier sizing calculations through semi-empirical correlations highlighted in the literature model as it is one of the few studies that discloses parameters for validation [26].

The versatility of HDH desalination is reflected in the different objectives for which models have been constructed. Many studies present a parametric analysis of a theoretical system for comparing different system configurations or showcasing different modeling methods [26,66,69,72,77]. However, there is a wide range of models that have been developed to analyze and optimize real life systems, including small experimental deployments [71,73,80]. Transient modeling approaches enable the simulation of HDH systems at variating conditions such as feed water changes due to weather [79] or energy supply variations such as solar power [78] or waste heat from refrigeration [81]. Finally, there are also cases that employ HDH modeling for statistics-based optimization [70].

3.1.4. Reverse Osmosis

Reverse Osmosis (RO) is the most widely used desalination method due to its relatively low energy consumption and adaptability for large scale production requirements. Pump energy consumption is considered as the main energy input to drive desalination in this process. The main component of a RO system is the membrane module, which in most cases contains a spiral-wound membrane used to filter product water high salinity feed. RO uses electricity as its energy source through a high-pressure pump. When the system pump exerts enough pressure on the feed side of the membrane to overcome the net pressure difference, which includes the hydraulic and osmotic pressures, water is forced through the membrane, resulting in a permeated product water and a leftover brine stream at a higher concentration. The RO metamodel is based on a single-pass, tapered arrangement system as shown in Fig. 5.

The RO process extracts water from a saline stream through physical separation as opposed to phase change; therefore, the osmotic pressure calculation becomes particularly important in modeling. Different studies present disparate assumptions in calculating colligative properties of saline water. Most published models assume linear dependence between osmotic pressure and salt concentration with a constant empirical coefficient of proportionality [82–84]. These approaches are based on van't Hoff's correlation, which involves temperature and salinity and is widely used in RO modeling [85]. Linearization, however, is mostly applicable to low salt content and can deviate at higher concentrations [86]. Other approaches consist in fitting a concentration-dependent regression to tabulated data [87]. The proposed RO metamodel employs a subroutine based on van't Hoff's expression in combination of other equations and approximations to expand the validity range [88].

Table 6 shows the relevant RO metamodel equations that are solved in a forward iterative algorithm by adding differential membrane elements to the system until the required desalination objective is achieved.

Like most RO models, our proposed metamodel employs a solutiondiffusion model that makes the water and salt fluxes proportional to the net force and concentration difference, respectively, across the membrane [89]. The proportionality constants in these equations are water and salt permeability coefficients that depend on the specific membrane and operation of the system. These parameters are not usually included in membrane catalogues and therefore the approaches to implementing Desalination 525 (2022) 115474

Table 5 HDH metamodel key equations.

S.A. Romo et al.

| Component | Equation | | Varia | bles | Ref. |
|--------------|--|------|-------------------------|---|------------|
| Dehumidifier | $M_a(h_{a2} - h_{a3}) = M_w(h_{w1} - h_{w0})$ | (13) | M_a h_{a2} h_{a3} | Air flow rate Moist air enthalpy Moist air enthalpy | [26] |
| | | | M_w | Intake water flow rate | |
| | | | h_{w1} | Saline water enthalpy | |
| | | | h_{w0} | Saline water enthalpy | |
| Humidifier | $M_a(h_{a2} - h_{a1}) = M_f c_p(T_{w3} - T_{w2})$ | (14) | M_f | Feed water flow rate | [26,77] |
| | | | c_p T_{w3} | Specific heat Brine | |
| | | | T_{w2} | temperature Inlet water | |
| Humidifier | $L_h =$ | (15) | L_h | temperature Humidifier | [26,72] |
| (sizing) | $\frac{M_f c_p M_a^2 (C_1 - C_2)}{C_s k A_h}$ | | C_1 | length Demister packing | |
| | | | C_2 | density Vapor velocity | |
| | | | L_p | Packing length | |
| | | | d_p | Packing diameter | |
| | | | C_s | Fitting parameter | |
| | | | k | Mass transfer coefficient | |
| | | | A_h | Cross- sectional area | |
| Heater | $M_f(h_{w, 2} - h_{w, 1}) = M_p \lambda_p$ | (16) | M_p | Motive steam flow rate | [26] |
| Dehumidifier | $U_c = 1719.4 +$ | (17) | $\lambda_p \ T_c$ | Latent heat Vapor | [24,45,65] |
| HTC | $3.2063T_c + 1.5971 \times 10^{-2}T_c^2 - 1.9918 \times$ | | | temperature at condenser inlet | |
| | $10^{-4}T_c^3$ | | U_c | Condenser heat transfer coefficient | |

these coefficients vary across the literature. It is common among published models to assume constant permeability coefficients [87]. These are often deduced from actual system measurements through regression analysis [82,83,85], or adjusted to match results from commercial simulation packages [84]. It is important to note that these coefficients tend to be strongly dependent on the feedwater characteristics, system specifications, and operational conditions, therefore these values are not

necessarily interchangeable among models.

The RO membrane blocks most salt ions from permeating; therefore, a high concentration layer is formed at the interface between membrane surface and the feed water stream. This phenomenon is called concentration polarization and can have significant effects on the water and salt fluxes through the membrane as they factor into a mass transfer coefficient through the membrane [90]. Concentration polarization is usually modeled as a factor given by the ratio of the wall-permeate and brine-permeate concentration differences through thin film theory [89]. This poses a challenge since the actual product concentration cannot not be known a-priori unless measured and regressed from an actual system. There are modeling cases in the literature that concentration polarization is not considered [91], or the value for product water concentration is assumed to simplify the equations [92]. In many cases, the models simplify the calculation by assuming a linear increase in brine concentration with respect to the flow path length and using a mass balance approach [83,84,87]. The RO metamodel incorporates different empirical correlations for calculating this mass transfer coefficient, which can be averaged or individually selected according to the membrane type and system setup [27,93,94]. In the model validation we choose the correlation that best fits the available data.

There are several analytical levels at which RO systems are modeled in the literature. A common approach to modeling single stage systems involves treating the flow channel as bulk [95-97]. Within this simplification there are several approaches, such as statistical-mechanical models, that require several fitting constants from experimental data [22,98], or solving for simultaneous equations in the simplified control volume [84,87]. Models based on empirical correlations, however, are only valid for the operating conditions, membrane modules, and plant configuration used in the statistical regressions, so they do not allow for flexibility in terms of modeling different desalination requirements or systems. Simplifying the system might not be appropriate for large, multi-stage systems since the effects of concentration polarization are diminished. More detailed analytical models use finite element approximations and follow an iterative calculation process through the discretized membrane elements [27,92]. Higher detail on fluid transport can be studied through CFD-based models [99]. The different modeling approaches and assumptions are tailored to specific modeling objectives. For instance, many studies use RO models to conduct parametric studies with different purposes such as exploring theoretical system tradeoffs [91,92,95], process optimization [84], or developing case studies with actual desalination plants [87]. In addition, RO models have been used to study transient effects through dynamic simulations [97]. Alternatively, numerical method-based models aim to explore more detailed and mechanistic modeling options that do not rely on common modeling assumptions [99].

3.1.5. Electrodialysis

Electrodialysis (EDS) is a desalination method that is still in the early phases of large-scale commercialization. The EDS process uses an

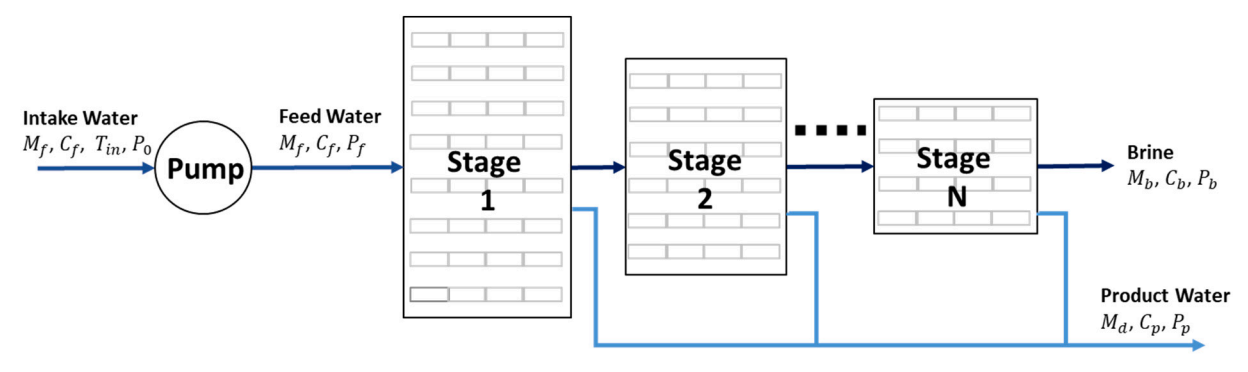


Fig. 5. RO process schematic.

Table 6RO metamodel key equations.

| Component | Equation | | Variables | | Ref. |
|----------------------------|--|------|----------------|---|----------------|
| Membrane permeation | $J_w = K_w[(P_b - P_p) - (\beta \pi_b - \pi_p)]$ | (18) | J_w | Water flux | [27,85] |
| | | | K_w | Water permeability | |
| | | | P_b | Feed (brine of previous element) pressure | |
| | | | P_p | Permeate pressure | |
| | | | β | Concentration polarization factor | |
| | | | π_b | Feed (brine of previous element) osmotic pressure | |
| | | | π_p | Permeate osmotic pressure | |
| Concentration polarization | J_w | (19) | Rej | Observed salt rejection | [27,89,97,100] |
| • | $\beta = Rejexp\left(\frac{1}{k_{cp}}\right) - Rej + 1$ | | k_{cp} | Mass transfer coefficient | |
| Local salt rejection | $eta = Rejexpigg(rac{J_w}{k_{cp}}igg) - Rej + 1$ $Rej = 1 - rac{C_p}{C_f}$ | (20) | C_p | Permeate concentration | [27,97] |
| | $Rej = 1 - \frac{\cdot}{C_f}$ | | C_b | Feed (brine of previous element) concentration | |
| Mass transfer coefficient | $D_T \setminus D_T \setminus D_{875} \setminus D_{10}$ | (21) | dH | Hydraulic diameter | [101] |
| | $k_{cp} = 0.023 \left(\frac{D_T}{dH}\right) (Re)^{0.875} (Sc)^{0.25}$ | | λ | Empirical multiplier | |
| | | (22) | ν | Flow velocity | [102] |
| | $k_{cp} = \lambda \left(\frac{D_T}{dH}\right) (Re)^{0.50} (Sc)^{1/3}$ | | 1 | Element length | |
| | $k_{cp} = 0.664 \left(\frac{D_T}{dH}\right) (Re)^{0.5} (Sc)^{0.33} \left(\frac{dH}{L}\right)^{0.5}$ | (23) | h | Channel thickness | [103] |
| | $k_{cp} = 0.664 \left(\frac{1}{dH}\right) (Re)^{0.5} (Sc)^{0.55} \left(\frac{1}{L}\right)^{0.5}$ | , , | D_{25} | Diffusivity of salt through membrane at 25 °C | |
| | $k_{cp} = 0.808 \left(\frac{6\nu D_{25}^2}{hl}\right) \frac{1}{3} \left(\frac{D_T}{D_{25}}\right) \frac{2}{3}$ $P_m = \frac{Q_f (P_f - P_0)}{2}$ | (24) | D_T | Diffusivity of salt at actual temperature | [93] |
| Pump | $Q_f(P_f-P_0)$ D_{25} | (25) | P_m | Motor power | [91] |
| - | $P_m = \frac{g(f)}{\eta_{pumn}\eta_{motor}}$ | | Q_f | Feed flow rate | |
| | · · pump · · motor | | P_0 | Intake pressure | |
| | | | η_{pump} | Pump efficiency | |
| | | | η_{motor} | Motor efficiency | |

electrical driving force to transport salt ions across ion selective membrane arrays. The lack of a thermal process and low fouling potential due to flow reversal ability make EDS an attractive option for desalination [104]. The process is mostly viable for low production capacity and low salinity ranges. In this desalination process, two different saline flows, a dilluate stream and a (saline) concentrate stream, flow into several channels in the EDS stack. An EDS stack contains many alternating anion and cation exchange membrane pairs, and the spaces in between are called cells. When a voltage is applied to the stack through a pair of electrodes located each end, negatively charged salt ions flow through the anion permeable membranes towards the cathode and are stopped by the cation permeable membranes. Conversely, positively charged salt ions flow through the cation permeable membranes towards the anion and cannot flow through the cells that contain anion permeable membranes. This process results in the formation of cells with alternating concentration where the dilluate and concentrate solutions are simultaneously desalted and concentrated, respectively, as shown in Fig. 6. The main energy consumption in the system occurs through the electrical input in the EDS stacks. Circulation pump energy is not considered in this analysis as it is insignificant in comparison t the operational conditions from the literature.

The EDS process involves ion transport within channels in the stack as a response to an electrical force; therefore, the electrical conductivity of the fluid is one of the most important thermophysical properties to consider. Some studies use a linear equation between conductivity and fluid concentration using ion conductance [28,105], while other studies

propose higher order numerical correlations [106,107]. There are also models that include temperature effects through regression approach [108]. It must be noted that for all the instances, the employed correlations are limited to relatively low concentrations, which corroborates the most common concentration ranges this method usually operates in. Table 7 describes the relevant EDS metamodel equations which are solved in a forward sequential algorithm.

The EDS process is constrained by the Limiting Current Density (LCD), which occurs at the maximum voltage for which water molecules begin to dissociate. Thus, if exceeded, it can result in a significant drop in overall efficiency of the system and increasing the risk of scaling [109].

This phenomenon occurs in the dilluate channel at the interface between the desalted stream and the membrane surface, therefore, it is highly dependent on the boundary layer formed which involves the specific flow and surface characteristics [110]. There are few studies that propose models that do not consider LCD explicitly; however, its effect is factored into their numerical correlations as a data-driven coefficient [105,107]. Thus, it must be noted that while there are several approaches to LCD modeling, these solutions are valid only on a case-bycase basis and might not be appropriate to be used interchangeably. In some studies, LCD is calculated through a polynomial regression [111,112]. Most EDS models in the literature, however, assume a power law relation that involves flow velocity and salt concentration and fit the equation to measured data from a bench system [113–115]. Some complex analytical solutions based on boundary layer analysis have been proposed; however, this still requiring the input of measured

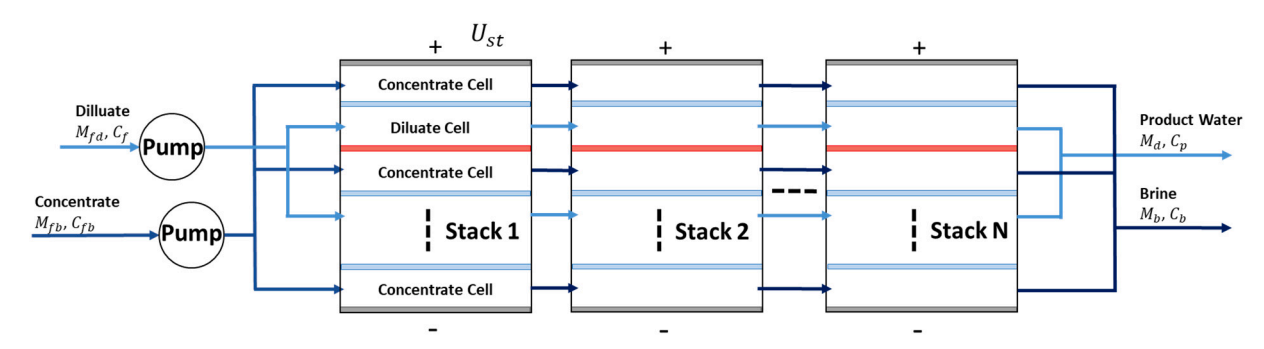


Fig. 6. EDS process schematic.

Table 7 EDS metamodel key equations.

| Component | Equation | | Variables | | Ref. | |
|--------------------------|---|------|--------------|-----------------------------|------|--|
| | | | i_{lim} | Limiting current density | | |
| | | | S | Safety factor | | |
| Limiting Current Density | $i_{lim} = saC_{\Delta}u^b$ | (26) | а | Regression constant | [28] | |
| Limiting Current Density | $u_{lm} = \mathfrak{suc}_{\Delta}u$ | (20) | C_{Δ} | Degree of desalination | [20] | |
| | | | u | Linear flow velocity | | |
| | | | b | Regression constant | | |
| | | | N_{cp} | Number of cell pairs | | |
| Cell pairs | | | Q_d | Product flow rate | [28] | |
| | $N_{cp} = \frac{Q_d}{\alpha w \Delta^* u}$ | (27) | α | Volume factor | | |
| | $\alpha w \Delta \dot{u}$ | | w | Cell width | | |
| | | | Δ | Cell thickness | | |
| | | | I_{st} | Stack current | | |
| Electrical current | $_{r}$ $zFQ_{d}C_{\Delta}$ | (28) | Z | Valence number | [28] | |
| Electrical current | $I_{ m st} = rac{z F Q_d C_\Delta}{\zeta N_{cp}}$ | (26) | F | Faraday constant | | |
| | • | | ζ | Current utilization factor | | |
| | | | L_{prac} | Flow path length | | |
| | | | C_b | Concentrate outlet salinity | | |
| | $(, (C_bC_f), \Lambda\rho C_{\Delta})$ | | C_f | Dilluate feed salinity | | |
| Stack | $\left(\ln\left(\frac{1}{C_{th}C_{d}}\right) + \frac{1}{\Delta}\right) z F C_{d} u \Delta \alpha$ | (29) | C_{fb} | Concentrate feed salinity | [28] | |
| Statik | $L_{prac} = rac{\left(lnigg(rac{C_bC_f}{C_f_bC_d}igg) + rac{\Lambda ho C_\Delta}{\Delta} ight)zFC_du\Deltalpha}{\left(rac{C_d}{C_h} + 1 + rac{\Lambda C_d ho}{\Delta} ight)l_{lim}eta\zeta}$ | (29) | C_d | Dilluate outlet salinity | | |
| | | | Λ | Equivalent conductivity | | |
| | , | | ho | Membrane area resistance | | |
| | | | β | Area factor | | |

parameters [116]. Our EDS metamodel calculates the LCD through a power law relation as the literature model provides the necessary coefficients and exponents that are usually undisclosed in other studies [28].

There are several differences in the computational approach between EDS models. The majority opt for defining a control volume for either a single EDS stack or multiple stacks in series and solving the transport equations as a bulk process [28,107,108,117]. Others maintain the large control volume in the EDS stacks but use numerical approaches that require iterations for a solution to converge [106,118]. A more recent modeling approach discretizes the EDS stack into finite elements and applies the modeling equations through the flow channel length [119]. Considering EDS modeling equations are largely based on empirical correlations that are tailored to specific operational conditions, it is unlikely yet that a single modeling approach can successfully represent other studies.

The EDS modeling approach and underlying assumptions are related to the modeling objective in each study. There are some cases for parametric analysis or optimization of a theoretical system [107,117], design of an actual plant [28], or dissemination of modeling approaches for alternate operational methods [106,120]. The latest studies propose new modeling methods with the aim of expand operational ranges or generalize applicability to a wider range of systems [108,119].

3.1.6. Capacitive Deionization

Capacitive Deionization (CDI) is a relatively new technology that

makes use of an electrochemical force to adsorb ions from aqueous solutions [121]. A conventional CDI system consists in a cell made by two parallel porous electrodes with a separator in between through which saline water flows. As shown in Fig. 7, during the charging phase, a voltage difference is applied and salt ions in the solution migrate into the electrical double layers that are formed along the inner surfaces of the porous electrodes [122]. Adsorbed ions are retained in the electrodes until the applied voltage is reversed or the electrodes are shorted. This releases the ions back into the saline water stream regenerating the electrodes for the next cycle [123]. Thus, desalination through CDI consists of alternating charging and discharging cycles in a CDI cell to produce an alternating desalted water and brine stream, respectively. There are several variations of CDI cell architecture. For cases where the flow is parallel to the electrodes configuration, it is common to implement ion selective membranes between the flow channel and the electrode, and there are also instances where the flow occurs perpendicular and through the electrodes [122]. Although CDI technologies remain largely experimental with a lot of theoretical work done in the field, we believe it is important to include them in this study to explore how it compares to benchmark operation of conventional desalination processes.

Modeling the mechanism through which ions are retained within the porous electrode is still a matter of ongoing research. The latest modeling approaches consider an electrical double layer composed of a constant ionic surface formed by the salt ions adherence to the electrodes, and a diffusive layer where the electric potential decreases

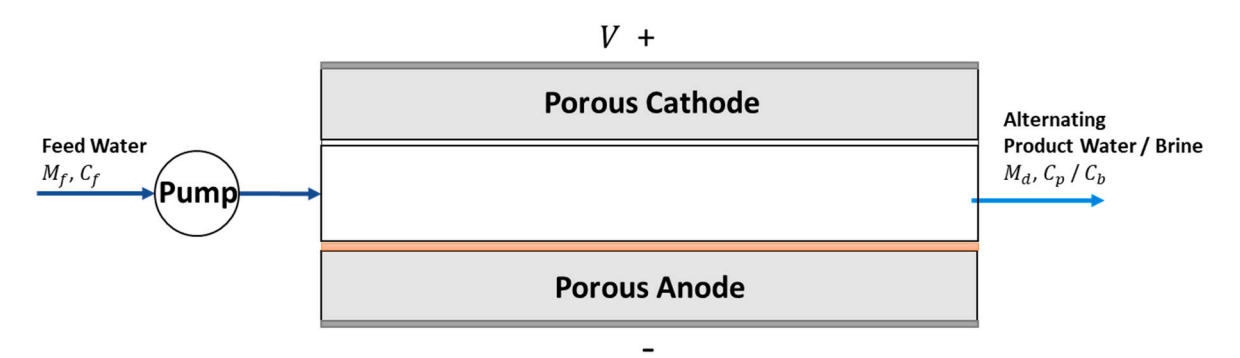


Fig. 7. CDI process schematic.

exponentially towards the center of the flow [124]. The implementation of electrical double layer theory in CDI is still under development, and there are several approaches in the literature models. Reduced-order models in the literature consider voltage drops across the whole CDI stack through a higher analytical resolution [11,125,126]. The subsequent tier in analytical resolution employ bulk modeling of the fluid without considering the boundary layer effects at the electrode interface [127]. The majority of models found in CDI, however, employ a mechanistic approach to electrical double-layer modeling [128–130].

CDI desalination is inherently a dynamic process as operation alternates between charging and discharging as desalination and concentration, respectively, occurs. There are different modeling approaches to considering time dependence at different spatial resolutions in the literature, and this is still a topic of current research. The literature presents design models that consider time marching only by executing the modeling algorithm at a system level through each time step [29,130]. Within this approach, some studies propose models that require measuring an experimental system and fitting equation parameters [127,128,131]. Other approaches discretize the flow channel into differential elements and execute the modeling algorithm through spatial iterations [129,132]. Mechanistic models employ numerical method schemes to iterate through discretized space and time [133].

CDI desalination is still in experimental stages, so therefore most models focus on mechanistic approaches at a fluid flow analytical scope that would help understand ion transport and concentration changes. The alternative approaches to modeling scope and methods cater to the particular objectives of the study. These include parametric optimization [130], dynamic modeling to investigate transient effects [127,134], determining electronic resistances across the stack [131], and the study of constant current or constant voltage operation [132,135]. On the other hand, there are several studies where generalized models are deployed with the purpose of modeling CDI at a system scope; for instance, exploring options of stack coupling for energy recuperation [129]. It is important to note that these objectives aim to advance the knowledge in CDI desalination and there is still not a robust system-level model although a modeling framework has been proposed [136] and generalized models have been used to determine contributions to energy consumption [29]. For this reason, we implement a generalized modeling approach in our metamodel which simplifies the CDI stack into an equivalent Randles circuit [29] where the ion exchange membranes, current collectors, and solution are modeled as a resistor with resistance R_1 , and the electrodes are modeled as a charging capacitor with fixed capacitance C and fixed resistance, R_2 , connected in parallel as shown in Fig. 8. The circuit is solved using a forward sequential algorithm for every timestep during charging and discharging. The variation in salt concentration in the product stream is calculated through the changes in R_1 at each timestep using the CDI metamodel equations described in Table 8. This assumption neglects energy of the circulation pump which is minimal in comparison to the energy input in the CDI stack at the operation conditions from the literature.

Table 8
CDI metamodel key equations.

| Component | Equation | | Variables | | Ref. |
|-----------------|--|------|------------------------|-------------------------------|------|
| Membranes, | $R_1 = s + \frac{l}{kA_s}$ | (30) | R_1 | Equivalent resistance | [29] |
| collectors, | 74. Ze | | S | Internal | |
| and solution | | | | resistance | |
| | | | 1 | Stack length | |
| | | | k | Electrical | |
| | | | | conductivity at | |
| | | | | time t | |
| Stack operation | | (31) | A_e | Electrode area Discharging | [29] |
| Stack operation | $t_{discharge} =$ | (31) | t _{discharge} | time | [29] |
| | $t_{charge} \left(\frac{1}{RR} - 1 \right)$ | | t_{charge} | Charging time | |
| | | | RR | Recovery ratio | |
| Stack | $V=I_1(R_2+$ | (32) | V | Applied | [29] |
| (charging) | R_1) – I_1R_2 exp | | | voltage | |
| | (.) | | I_1 | Applied | |
| | $\left(\frac{-t}{R_2C}\right)$ | | R_2 | current Equivalent | |
| | $(\kappa_2 c)$ | | N ₂ | electrode | |
| | | | | resistance | |
| | | | t | Operation | |
| | | | | time | |
| | | | C | Equivalent | |
| | | | | electrode | |
| | | | | capacitance | |
| Stack | $V_{discharge} = -$ | (33) | $V_{discharge}$ | Discharge | [29] |
| (discharging) | | | | voltage across | |
| | $Vexp\left(\frac{-t}{R_{\cdot}C}\right)$ | | | CDI stack | |
| | (R_tC) | | R_t | Equivalent stack | |
| | | | | resistance | |
| | | | | resistance | |

3.2. Simulation framework

Standardizing desalination modeling algorithms involves defining common sets of inputs and outputs for all desalination models. There is a notion in previous studies of defining an operational range for desalination processes according to the production flow rates and feed water concentrations [2,5,6,9]. These parameters impose practical limits of operation and therefore would be appropriate to group them as common inputs to the models. Furthermore, these parameters represent the same physical concept in all methods and therefore can be directly compared. Defining which parameters can be compared and the order of relevance in which analysis should be directed is the basis for the proposed cross-comparison framework. Therefore, we propose a standard classification of inputs and outputs which include the General, Family and Specific analytical hierarchies. Such standardization resolves the computational order discrepancies in existing models and thus enables cross-comparison.

3.2.1. General variables

Any desalination process intakes a feed stream of saline water (M_f) at a certain intake temperature (T_{in}) with salt concentration (C_f) and

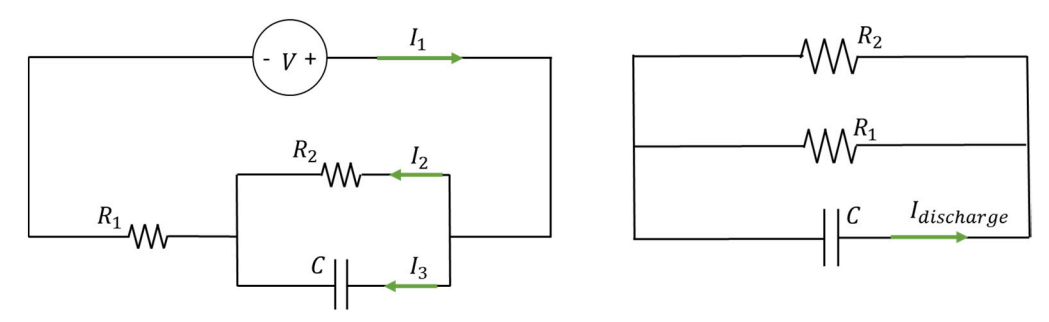


Fig. 8. Randles circuit equivalent of a MCDI system charging (left) and discharging (right).

through an energy input extracts a product water stream (M_d) with negligible salt concentration (C_d) and a brine stream flow rate (M_b) with a higher salt concentration (C_b) . Therefore, a mass balance for water can be written as:

$$M_f = M_d + M_b \tag{34}$$

And salt:

$$M_f C_f = M_d C_d + M_b C_b \tag{35}$$

Eqs. (34) and (35) hold for any desalination method.

The molecular transport desalination processes, RO, EDS, and CDI, are driven by either an external physical or electrostatic force inputted through a pair of electrodes or a pump. This force must be high enough to overcome intermolecular forces, such as osmotic pressure or intermolecular electrostatic attractions that are higher than those of pure water due to the presence of salt. This separation results in two liquid streams, the product stream with a lower salt content and the brine stream with a higher salt concentration. Thermal desalination systems, including TVC, MED, and HDH, extract water from the saline feed through a phase change, therefore, the product concentration can be assumed zero and the salt balance reduces to:

$$M_f C_f = M_b C_b \tag{36}$$

A recovery ratio (RR), which indicates the proportion of product water flow rate (M_d) recovered from feed water flow rate (M_f), can be defined for all desalination processes such that:

$$RR = \frac{M_d}{M_f} \tag{37}$$

The parameters M_f , M_b , M_d , C_f , C_b , C_d , T_{in} , and RR form part of the "General" parameter hierarchy. This category corresponds to variables that are numerically equivalent in all desalination methods and therefore can be directly compared with one another.

3.2.2. Family variables

The proposed framework for cross-comparison between distinct desalination processes takes into first consideration the clear distinction between thermal desalination processes, which use thermal energy to induce a phase change to separate water from salt, and molecular transport processes, which conversely use an external force to separate water and salt through molecular dynamics. All desalination processes have a power input (P_{des}) to the system required to overcome intermolecular attractions so that separation can occur. This input can be either thermal, electrical, or mechanical energy depending on the method and can be normalized by M_d to obtain an energy intensity of desalination:

$$E_{des} = \frac{P_{des}}{M_d} \tag{38}$$

It is important to note that electrical and thermal power cannot be directly compared as they are region and market dependent. Therefore, although the numerical value of E_{des} describes the same parameter within desalination, it must be considered as a Family Variable. Future research can investigate appropriate conversion factors to complement the direct comparison of General desalination-related operation variables such as flow rates, salinities, and end performance ratios as presented in this study.

Thermal desalination processes including TVC, MED, and HDH desalination in this study are driven by the heat released from condensation of motive steam inputted to the system at a pressure P_s . This must supply enough heat to evaporate water from the saline feed the produced vapor and must later be condensed using cooling water or brine acting as a heat sink. The nature of this process suggests metrics for cross-comparison that include motive steam flow rate, heat exchanger area, and cooling water flow rate. The relevant metrics of performance are the Gain Ratio (GR) and the Specific Cooling Water (sM_{cw}):

$$GR = \frac{M_d}{M_p} \tag{39}$$

$$sM_{cw} = \frac{M_{cw}}{M_d} \tag{40}$$

where M_p is the motive steam flow rate, and M_{cw} is the cooling water flow rate. The parameters P_s , M_p , GR, and sM_{cw} are numerically equivalent only within the desalination methods corresponding to the thermal family. Therefore, it is appropriate to cross-compare these metrics and parameters directly only between TVC, MED, and HDH. The formal separation of these desalination families is further corroborated by the thermophysical properties involved in the desalination process. Thermal desalination models employ, for instance, specific heat capacities, latent heat of evaporation, and boiling point elevation while molecular transport models involve other properties, such as osmotic pressure and conductivity.

3.2.3. Specific hierarchy

The remaining parameters inherent to each desalination method form part of the Specific Hierarchy. These variables are numerically compatible only within the specific desalination method and cannot be cross compared with different methods as they are not related. This hierarchy becomes particularly useful when analyzing different operation conditions for the same desalination system. The full list of specific parameters corresponding to each model are given in Table 9 of the following section.

3.2.4. Cross-comparison enabling simulation framework

The proposed simulation framework imposes that cross-comparison between different desalination technologies can only occur across equal hierarchy levels for which the parameters have the same numerical and physical meaning. It is necessary to maintain constant inputoutput structures in the metamodels to enable a direct crosscomparison at the different hierarchy levels and facilitate sequential algorithm solution. All desalination processes can be cross-compared at the General Hierarchy level, while only models of the same desalination family can be cross-compared across the Family Hierarchy level. Finally, only variations within the same desalination process can be compared using data corresponding to the Specific Hierarchy level as it has the same representation across technologies and thus allows for fair and meaningful and fair comparisons. It is important, however, to consider parameters that are incompatible for cross-comparison but could still provide valuable insight on system operation and performance. For instance, when comparing two different methods, there will not be direct cross-comparison of specific variables; however, identifying them can yield valuable information about the system that can factor into an indirect comparison. Table 9 summarizes the inputs and outputs for each model under the proposed analytical hierarchy structure.

4. Discussion

In the first part of this section, we deploy the proposed simulation framework using the base representative literature model inputs in a high-level, cross-comparative analysis. The similar energy consumption patterns observed, even though the operational regimes are disconnected, justify the framework as appropriate for joining seemingly disconnected models. The similar operation patterns throughout the six studied desalination processes suggest that conservation laws form a theoretical performance curve that represents ideal operation. However, actual performance depends on system design and operating conditions, which in this analysis, are expressed as energy intensity patterns based on meta-analysis of the literature. The performance curves provide evidence that a system can operate in sub-optimal regimes.

For the second part of this section, we apply the framework in a full

Table 9Input and output hierarchy for cross-comparison

| Hierarchy level | Parameters | | | | | | | | |
|---|---|---|--|---|--|---|--|--|--|
| 1. General | Inputs: | | | Outputs: | | | | | |
| Parameters that are numerically compatible among all desalination technologies | • Target product Flow rate, M_d (kg/s) • Intake Salinity, C_f (g/kg) • Intake Temp. T_{in} (°C) | | | Product Flow rate, M_d (kg/s) Feed water flow rate, M_f (kg/s) Brine flow rate, M_b (kg/s) Product water salinity, C_p (g/kg) Brine salinity, C_b (g/kg) Recovery ratio, RR | | | | | |
| 2. Family Parameters that are | • | | | Molecular transport desalination Inputs | | | | | |
| among desalination technologies within the same family | Motive steam press Outputs | sure, P_s (kPa) | | • Target recovery ratio, a Outputs | RR | | | | |
| | Specific energy (th Motive steam flow Gain ratio, <i>GR</i> | rate, M_p (kg/s) | | Specific energy (electric | ical), E_{des} (kWh/m ³) | | | | |
| | Sp. cooling water in | | - | | PD 0 | 00.4 | | | |
| 3. Specific Parameters that are valid | TVC | MED Inputs | HDH Inputs | RO | EDS | CDI Inputs | | | |
| only with a particular | Inputs | Inputs | inputs | Inputs | Inputs | inputs | | | |
| desalination method and is not compatible with any other | Operating temperature, T_ν (°C) Cond. area, A_c (m²) Compression ratio, CR Condenser effectiveness, η_c Outputs Evap. area, A_e (m²) Sp. Area, sA, (m²/(kg/s)) | Top brine temp. Tbt (°C) Last effect brine temp. Tb (°C) Feed water temp. Tf (°C) Brine salinity, Cb (g/kg) Outputs Cond. area, Ac (m²) Sp. Area, sA, (m²/(kg/s)) | Heater outlet air temp., T_{high} (°C) Hum. air inlet temp., T_{a1} (°C) Humidifier outlet air temp., T_{a2} (°C) Condenser outlet air temp., T_{a3} (°C) Hum. air inlet rel. hum. φ₁ Humidifier outlet air rel. hum. φ₂ Condenser outlet air rel. hum. φ₃ Feed water flow rate, M_f (kg/s) Condenser outlet water temp. T_{w1} (°C) Cond. HT coeff. U_c (kW/m²·c) Humidifier cross-sectional area, A_h (m²) Vapor mass transfer coefficient, k (kg/(sm³)) Outputs Cond. area, A_c (m²) Hum. Height, L_h (m) Air mass flow rate, M_a (kg/s) Total intake water flow rate, | Feed pressure, Pf (bar) Feed velocity, vf (m/s) Permeate pressure, Pp (bar) Module length, l (m) Channel width, h (mm) Module head loss, hl (bar) Module design velocity, vo (m/s) Membrane water permeability at 25 °C, K_{w25} L/(m².h.bar) Membrane salt permeability at 25 °C, K_{s25} (m/h) Temperature coefficient for water transport, K_{wt} (K) Temperature coefficient for salt transport, K_{st} (K) Outputs Number of stages, N_{stage} Number of modules, N_{modules} Membrane area, A_m (m²) Average water flux, J_w (L/(m²h)) | Product Concentration, C_d (g/kg) Linear flow velocity, u (m/s) Cell thickness, del (m) Cell width, w (m) Length per stack, L_{st} (m) Anion selective membrane resistance, ρ_a (Ohm.m²) Cation selective membrane resistance, ρ_c (Ohm.m²) LCD Constant, a (A. sʰm(1-b)/keq) LCD Constant, b Safety factor, s Volume factor, α Area factor, β Current utilization factor, ζ Outputs Concentrate feed mass flow rate, M_{fb} (kg/s) Concentrate feed concentration, C_{fb} (g/kg) Stack current, I_{st} (A) Stack voltage, U_{st} (V) Number of cell pairs, N_{cp} Number of Stacks, N_{st} | Normalized Current, I_{norm} (A/m²) Normalized Capacitance, C_{norm} (F/g) Normalized Internal resistance, s_{norm} (Ohm.m²) Normalized electrode resistance, R₂, norm (Ohm.m²) Electrode area density, m (g/m²) Charging step time, t_{charge} (s) CDI Stack volume, V_{cdi} (L) Channel thickness, l (mm) Charge efficiency, η_{charge} Discharging efficiency, η_{discharging} Max. Salt adsorption capacity, SAC (mg/g) Electrode area, A_e (m²) Outputs Desorption Capacity, (%) Max. Voltage, (V) | | | |

cross-comparative study between MED and RO; the desalination methods that currently have one of the largest market shares in seawater desalination, greatest maximum production capacity per unit, and highest technology growth trends [137]. Furthermore, we chose MED and RO to highlight that new desalination technologies must outcompete these processes in terms of operation and costs. The resulting cross-comparative analysis highlights that MED has energy consumption that is an order of magnitude greater than that of RO but uses a different type of energy. Such difference is justified by the cost of energy and maintenance for MED which must be an order of magnitude smaller than RO

for it to be competitive. The results help define a technical benchmark that upcoming desalination technologies must overcome in order to be competitive.

4.1. Application of the analytical framework in intended operation of desalination methods

Fig. 9 shows the distribution of M_d and C_f values collected from the reviewed literature. We consider operation points from studies that describe an actual desalination plant, model, or bench-scale system.

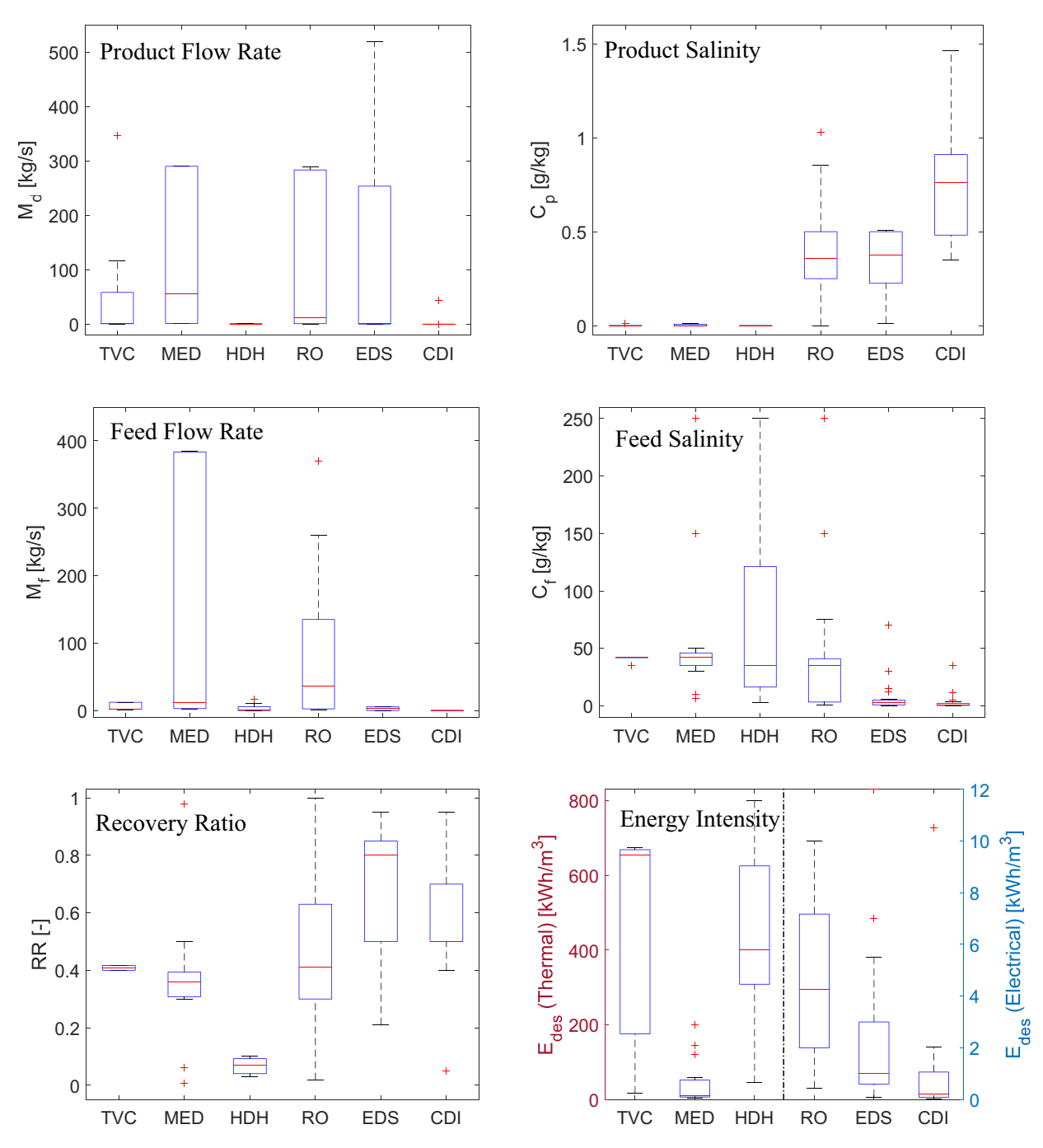


Fig. 9. Distribution of operation parameters in the literature for each desalination method.

Each study does not necessarily disclose all these parameters; therefore, the resulting median points only suggest typical operation from the literature. The meta-analysis shows that thermal desalination methods have a very similar C_f median with an average of 38.5 g/kg. Conversely,

EDS and CDI in the molecular transport methods have close C_f medians with an average of 1.74 g/kg. RO is the only molecular transport desalination method with instances in the literature that spans from molecular desalination to thermal desalination feed salinity ranges.

Table 10Outputs overview of cross-comparative simulations at case study operation points.

| Method | M_f [kg/s] | C_f [g/kg] | C_p [g/kg] | M_d [kg/s] | RR [-] | E_{des} [kWh/m ³] | M_b [kg/s] | C_b [g/kg] |
|--------|------------------------|--------------|--------------|----------------------|--------|---------------------------------|----------------------|--------------|
| TVC | 1.360 | 35 | 0 | 0.5787 | 0.43 | 239.9 | 0.7811 | 60.9 |
| MED | 366.9 | 46 | 0 | 137.9 | 0.38 | 66.37 | 234.4 | 72 |
| HDH | 16.87 | 35 | 0 | 1.156 | 0.069 | 486.5 | 15.48 | 38.2 |
| RO | 3.472 | 2 | 0.023 | 2.087 | 0.60 | 0.9099 | 1.383 | 4.99 |
| EDS | 5.401 | 3.5 | 0.35 | 4.051 | 0.75 | 0.3688 | 1.360 | 13.0 |
| CDI | 6.138×10^{-5} | 2 | 0.70 | 6.138×10^{-5} | 0.50 | 0.5594 | 6.138×10^{-5} | 2.54 |

Unsurprisingly, product salinity is negligible for the thermal processes while the molecular transport methods typically result in concentrations around the potable water limits of 0.6 g/kg. The distributions show that generally MED and RO can achieve similar product flow rates from the highest feed salinity levels while incurring in the lowest E_{des} .

Table 10 shows the metamodel simulation results using the most representative models as particular case studies from the literature. These could be considered optimal operation conditions. Thermal desalination methods show significantly greater energy intensity and lower recovery ratios but higher feed salinities than the molecular transport methods.

Fig. 10 shows the simulation points and the operation ranges from the meta-study. The system performance is summarized by recovery ratio and energy intensity where desirable operation is located close to RR=1 and lowest E_{des} . The molecular transport desalination methods show on average better performance as they achieve high recoveries with the lowest salinity values. MED and CDI exhibit typical recovery ratios but at a higher energy intensity. TVC has smaller energy intensity but also smaller water recovery. A limitation in this approach is that neither RR nor E_{des} captures the degree of desalination in the feeds stream, and a better metric could include E_{des} be normalized by $(C_f$ – $C_{\rm P}$). This, however, cannot be conducted with the range values from the meta-study as they do not correspond to a single desalination system constrained by mass transfer and energy equations. Specific recovery ratios, energy intensity, and other important parameters can be calculated using the metamodels for a given desalination system. Comparison to typical operation can help decision making between desalination methods or identify cases suboptimal operation, and simulation can provide more valuable insights into the tradeoffs within a system.

Fig. 11 shows the resulting surfaces formed by the response of energy intensity (E_{des}) to changes of $\pm 20\%$ in M_d and C_f from the base case operation described in the most representative model for each desalination method. The magnitude of a representative parameter of the system's size is represented by the diameter of the gray circles included in each point within the surface. All desalination technologies follow a similar sensitivity to variations M_d and C_f regardless of the operational space they were designed for and independent from the physical phenomena that drives salt and water separation.

The TVC surface shown in Fig. 11.A is the exception to the direct proportionality between C_f and E_{des} presented in other desalination technologies. In this analysis, the compression ratio (CR) is always fixed at 1.85, and the motive steam pressure (P_s) remains constant at 572 kPa according to the reference model inputs. The motive steam flow rate

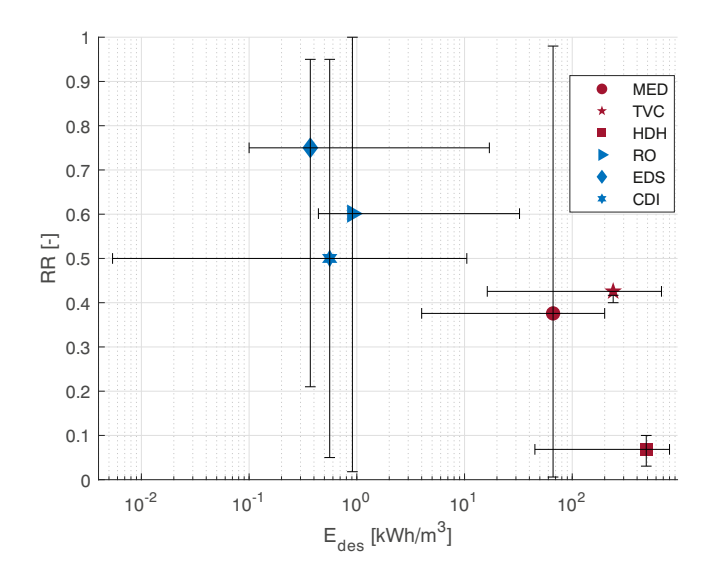


Fig. 10. Operational map: RR and energy intensity (with operation ranges from Fig. 9)

input to the system (M_p) must be adjusted to supply the required energy for desalination. There is a very small increase of the required M_p in response to increasing C_f . A greater C_f elevates the boiling point of the solution; however, this additional energy demand is compensated for by recirculating some of the produced steam as entrained steam into the thermoejector. The saturation temperature of the entrained steam increases in response to the boiling point elevation. Thus, the implementation of a thermocompressor stabilizes the energy demands of the desalination system with respect to changes in C_f . Since the entrained steam flow rate is adjusted to supply the required energy, the expansion ratioand the mass ratio remain constant, and the output is always superheated steam. The system size follows a similar response pattern to changes M_d as larger flow rates demand larger systems to provide enough surface area for the required heat exchange.

The implemented simulation framework imposes common design constraints across all the desalination metamodels. There is an exception in the HDH metamodel because, unlike the other metamodels, HDH has M_f as an input with a numerical value much greater than M_d that remains constant through all the calculated points in the surface. Thus, a constant, large saline water stream is unnecessarily heated independent from the specified M_d , resulting in a large, constant energy consumption that becomes smaller when normalized by larger values of M_d as shown in Fig. 11.C. The model energy consumption does not present a strong response to changes in C_f because the additional energy required due to the variation in the specific heat capacity is insignificant within the studied C_f range in comparison to the energy involved in heating the bulk flow of the specified M_f stream. The marker diameter is scaled according to the dehumidifier area, which positively correlates to the product flow rate as the other desalination technologies.

The intended operational surface for MED, RO, EDS, and CDI presents similar responses of a direct proportionality between feedwater salt concentration and energy intensity as shown in Fig. 11.B, D, E, and F. This agrees with the response of colligative properties: boiling point elevation for MED, osmotic pressure for RO, and electrochemical potential for EDS and CDI to changes in salt concentration. Practically, energy intensity (E_{des}) only depends on C_f is the in these desalination models. Conversely, E_{des} does not show a significant dependence on M_d ; instead, the product water flow rate drives the system size: condenser area for TVC and MED, dehumidifier area for HDH, membrane area for RO, and theoretical (not rounded) number of cell pairs for EDS and electrode area for CDI.

Advantages in some desalination methods lie on the practical limits to the system size, such as fouling or scaling potential, maintenance, and space availability as well as the quality and type of energy available on site to run the process. It is particularly evident in the molecular transport processes, whose representative cases have similar C_f , M_d and E_{des} magnitudes, that the advantages corresponding to system size are associated to the system's capital costs. Constraints indicated by the energy intensity of each process are associated to energy availability and cost. For instance, the magnitudes of energy intensity become irrelevant for the practical deployment of MED and HDH as these systems can be optimized to run on low-grade steam. TVC, on the other hand, requires high-grade steam which can incur higher operating costs. Finally, RO, EDS, and CDI use electricity, which is the most refined form of energy between these desalination methods and depending on the market and location, could be significantly more expensive.

4.1.1. Modeling regimes

The scalability of both the actual desalination methods and the corresponding models play a key role in dictating which can handle specific M_d and C_f ranges and therefore pose limitations in their deployment. The MED and RO processes are modular, as system size can be easily increased by adding an additional effect or stage to increase the heat transfer or membrane area, respectively, and adjusting the corresponding operation conditions to satisfy production requirements. Furthermore, these metamodels do not rely on numerical correlations

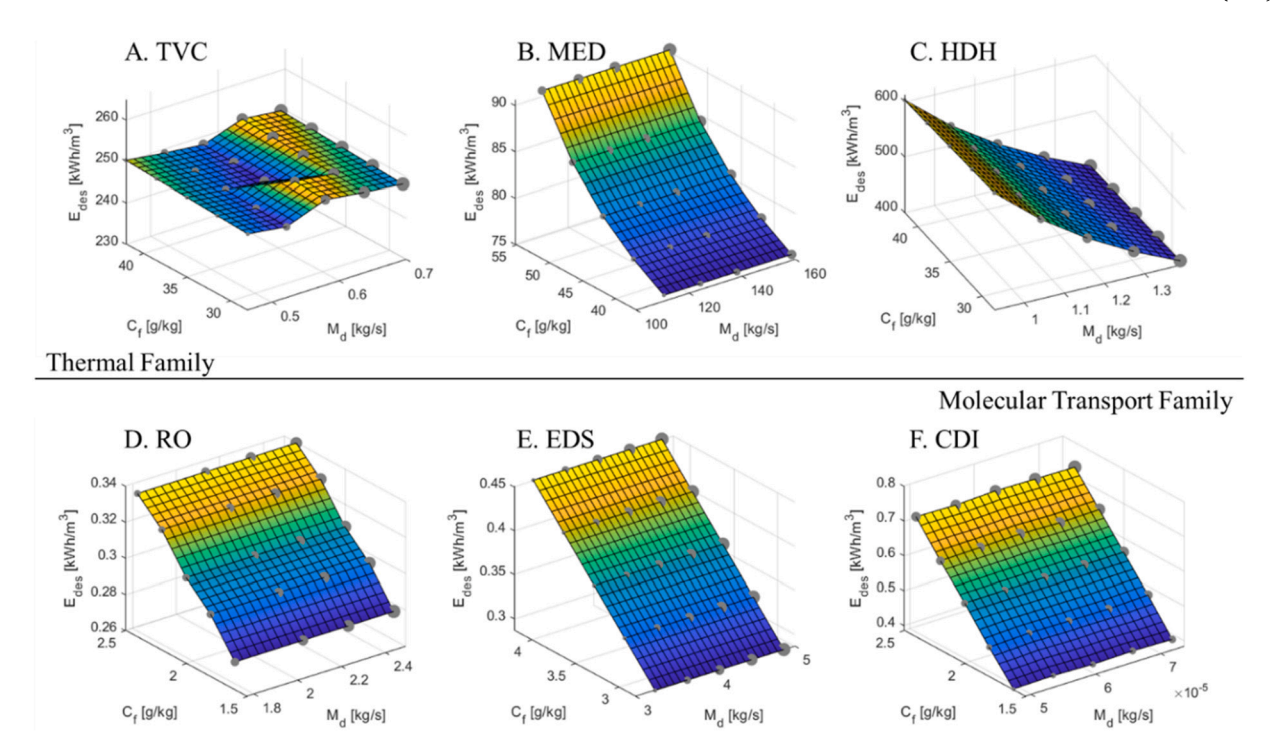


Fig. 11. Surface plots at $\pm 20\%$ from the design point for different desalination methods, all plots are optimized to minimize system size. (A): TVC – base case ($M_d = 0.5787$ kg/s, $C_f = 35$ g/kg) [24], (B) MED – base case ($M_d = 137.9$ kg/s, $C_f = 46$ g/kg) [25], (C) HDH – base case ($M_d = 1.156$ kg/s, $C_f = 35$ g/kg) [26], (D) RO – base case ($M_d = 2.087$ kg/s, $C_f = 2.0$ g/kg) [27], (E) EDS – base case ($M_d = 4.051$ kg/s, $C_f = 3.5$ g/kg) [28], (F) CDI – base case ($M_d = 6.138 \times 10^{-5}$ kg/s, $C_f = 2.0$ g/kg) [29].

that constrict them to a specific operational point. The other metamodels, on the other hand, present limitations in the validity of the correlations used to model key components such as the thermoejector in TVC, the humidifier in HDH, the limiting current density in EDS, and the equivalent resistances in CDI. It must be noted that most of these correlations are regressed from measured data valid for the specific component at the specific operational conditions and extrapolating to different C_f and M_d ranges might not be appropriate.

The operational regime plots in Fig. 11 include a $\pm 20\%$ deviation from the intended operational point that the literature model is designed for. It is important to highlight that even with this expanded operational ranges, the desalination models present no overlap in M_d . Specifically, the smallest range corresponds to CDI, which is found as a bench scale system with a M_d ranging from 4.9×10^{-5} to 7.4×10^{-5} kg/s. Then, there is a large gap of four orders of magnitude for the M_d ranges where most of the models for small scale systems operate without any intersection. TVC ranges from 0.46 to 0.69 kg/s, HDH from 0.92 to 1.39 kg/s, followed in increasing order by RO with an M_d range from 1.66 to 2.49 kg/s and EDS with a range from 3.24 to 4.86 kg/s. Finally, the operational range for MED is an order of magnitude greater ranging from 110 to 159 kg/s. On the other hand, the simulations present significant overlap in C_f . CDI and RO have complete intersection of C_f values ranging from 1.6 to 2.4 g/kg. This is followed by EDS with a C_f range from 0.29 to 4.2 g/kg. TVC and HDH have a complete intersection of C_f ranging from 28 to 42 g/kg. Finally, the MED simulations have partial intersection of about 37% with TVC and HDH because it ranges from 36.8 to 55.2 g/kg.

It is important to emphasize that these ranges specify the operational ranges for the representative literature models and not the possible operational range for each desalination method. Further research within each desalination method is required to find more accurate correlations that are applicable in wider operational ranges to minimize the modeling range gaps. All desalination models exhibit similar responses to variations of C_f and M_d and are observed despite the completely different operational ranges that each simulation case presents.

Therefore, the second part of this analysis deploys the proposed simulation framework and evaluates performance of the desalination methods within similar operational ranges. The models for CDI and EDS remain highly experimental while TVC and HDH are intended for very low production rates imposed by practical constraints that are not inherent to the desalination process. MED and RO are the most scalable technologies for both actual systems and theoretical modeling. Given that these two technologies are the predominant desalination processes in the desalination market, analyzing their performance at low, middle, and high C_f and M_d ranges would set an appropriate benchmark in both modeling capabilities and desalination efficiency that other technologies would compete with.

4.2. Cross-comparative simulation in common operational spaces

The first step for a fair assessment of MED and RO desalination performance is defining common operational conditions for deploying the developed simulation framework. The notion of classifying models according to a Low, Normal, and High production capacity has been previously documented among the thermal desalination processes [6]. We deploy the metamodels using C_f values of 2, 18, 35, and 50 g/kg for this study, which correspond to the limit for conventional irrigation, brackish water, sea water and brine processing, respectively. At each salinity level, we simulate product water flow rates of 2.3, 70, 138, and 1157 kg/s which correspond to common ranges for bench scale systems, industrial processing, municipal and large-scale systems, respectively. The feed water temperature is maintained at 24 °C for all the simulations. For each RO simulation case, the model attempts the maximum recovery ratio RR while minimizing feed pressure P_f . On the other hand, the MED simulations maintain a constant P_s at 31.2 kPa while minimizing the required steam flowrate M_p . Brine salt concentration C_b is fixed at 72 g/kg for all operational MED regimes. This limit corresponds to the maximum solubility limit of CaSO4 at common parallel feed MED operating temperatures [138]. At each $[C_f, M_d]$ regime (16 total), variations of $\pm 5\%$ and $\pm 10\%$ in both C_f and M_d (total of 25 simulations per

Table 11 Cross-comparative simulation results.

| | | MED | | | | | RO | | | | |
|-----------------------|--------------|--------------|--------------|--------------|--------|--|--------------|--------------|--------------|--------|--|
| M _d [kg/s] | C_f [g/kg] | M_b [kg/s] | C_b [g/kg] | C_p [g/kg] | RR [-] | E _{des, th} [kWh/m ³] | M_b [kg/s] | C_b [g/kg] | C_p [g/kg] | RR [-] | E _{des, el} [kWh/m ³] |
| 2.3 | 2 | 0.065 | 72 | 0 | 0.97 | 68.5 | 0.14 | 45 | 0.05 | 0.95 | 3.3 |
| | 18 | 0.76 | 72 | 0 | 0.76 | 70.7 | 0.73 | 86 | 0.25 | 0.78 | 4.5 |
| | 35 | 2.2 | 72 | 0 | 0.53 | 75.2 | 2.0 | 90 | 0.53 | 0.57 | 6.5 |
| | 50 | 5.7 | 72 | 0 | 0.32 | 86.5 | 4.0 | 90 | 0.90 | 0.39 | 1.2 |
| 70 | 2 | 2.0 | 72 | 0 | 0.97 | 68.5 | 4.2 | 42 | 0.05 | 0.95 | 3.3 |
| | 18 | 23 | 72 | 0 | 0.76 | 70.7 | 27 | 86 | 0.32 | 0.77 | 4.5 |
| | 35 | 67 | 72 | 0 | 0.53 | 75.2 | 59 | 88 | 0.53 | 0.57 | 6.5 |
| | 50 | 175 | 72 | 0 | 0.32 | 86.5 | 126 | 90 | 0.90 | 0.39 | 1.2 |
| 138 | 2 | 3.9 | 72 | 0 | 0.97 | 68.5 | 8.5 | 43 | 0.09 | 1.0 | 3.3 |
| | 18 | 46 | 72 | 0 | 0.76 | 70.7 | 45 | 89 | 0.26 | 0.78 | 4.5 |
| | 35 | 132 | 72 | 0 | 0.56 | 75.2 | 120 | 89 | 0.53 | 0.57 | 6.5 |
| | 50 | 343 | 72 | 0 | 0.32 | 86.5 | 241 | 89 | 0.90 | 0.39 | 1.5 |
| 1157 | 2 | 33 | 72 | 0 | 0.97 | 68.5 | 76 | 47 | 0.13 | 1.0 | 3.3 |
| | 18 | 382 | 72 | 0 | 0.77 | 70.7 | 348 | 83 | 0.25 | 0.78 | 4.5 |
| | 35 | 1109 | 72 | 0 | 0.53 | 75.2 | 963 | 88 | 0.52 | 0.57 | 6.5 |
| | 50 | 2888 | 72 | 0 | 0.32 | 86.5 | 1951 | 81 | 0.89 | 0.38 | 3.3 |

 $[C_f, M_d]$ pair) to account for variations that can occur in actual operation. Table 11 shows the results of the cross-comparative simulation, $[C_f, M_d]$ pair results are averaged in this analysis.

4.2.1. General hierarchy

Following the proposed cross-comparative framework, we first analyze the parameters within the General Hierarchy. The variables M_d , C_f , and T_{in} are fixed for MED and RO simulations within the same operational space. The motive steam pressure (P_s) remains constant for all MED simulations, and the motive steam flow rate (M_p) is optimized to supply enough heat for evaporation.

Fig. 12 shows the fitted linear regression recovery ratio for different feed water salt concentrations and different product flow requirements. The metamodels consistently find an optimum system performance for most of the simulation cases. The RO metamodel shows a small numerical instability at 2 g/kg feed salinity and 1157 kg/s resulting from the mass transfer coefficient calculation at those opposing extreme values. Future research would be required to produce general, unified mass transfer coefficient correlations. The results show that optimized MED and RO systems can achieve similar RR at low salinities. At higher concentrations, however, RO consistently shows higher RR values than MED with the largest difference being 10% at 50 g/kg. For both MED and RO, the system can extract less water as feed higher salinity increases while incurring in greater energy intensity.

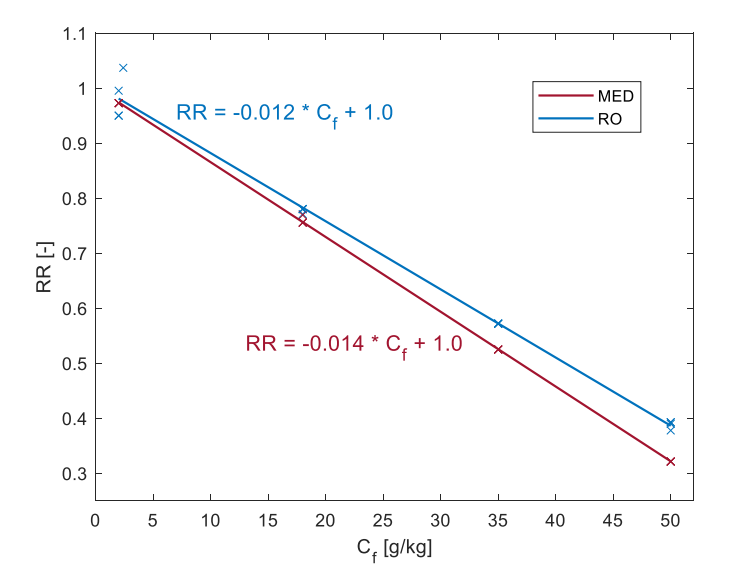


Fig. 12. Recovery ratio for RO at different feed salinities.

The average RR for all M_d scenarios can be approximated an inverse linear relationship to C_f which define optimal mass transfer capabilities. Ideal recovery can be described as a linear relationship with slopes of -0.012 and -0.014 for RO and MED, respectively, and an intercept of 1.0. In the case of MED, greater feed water concentrations lead to higher boiling point elevation. The operating temperatures of the system, however, are constrained by the temperature of motive steam and thus RR decreases for higher C_f . Conversely in the case of RO, this tradeoff occurs because greater concentrations lead to higher osmotic pressure to overcome by the high-pressure pump. Operating pressure is constrained by the maximum allowable pressure in the membrane module to prevent membrane rupture. The total drop in recovery ratio from the lowest to highest C_f values is about 60% for RO and almost 70% for MED. The regressed intercept is 1.0 suggesting that, theoretically, zero salinity levels would make full recovery possible.

Both MED and RO have a similar response of M_b to changes in C_f at all the studied M_d regimes. A direct proportionality is maintained for which the greater C_f results in larger brine production. At the M_d range between 2.3 and 138 kg/s, MED and RO have comparable brine production for all C_f values. However, at higher production rates of 1157 kg/s this similarity only holds up to 35 g/kg feed concentration. At the higher C_f ranges, MED shows significantly higher M_b values that can be about to 50% greater than the magnitude of M_b in RO. This is an important difference to consider as brine disposal can have negative environmental effects and result in expensive treatment processes.

Brine concentration in MED is constant at 72 g/kg as it is imposed in the system design as a safe maximum salinity limit to prevent fouling. On the other hand, RO presents lower C_b values for lower concentrations up to brackish water ranges. The operation conditions for MED and RO are dictated by solubility limits of salt to prevent fouling or scaling. From a modeling standpoint, brine concentration in MED can be defined a priori based on solubility limits of salts in the feed water stream [138]. RO, on the other hand, requires iterative simulations because solubility limits occur at membrane interface where concentration polarization takes place [139]. The resulting brine concentrations in RO are not consistently proportional to the magnitude of M_d because the model employs an iterative procedure involving discrete increments of membrane area. For RO cases of greater salinity, the discharged brine can have concentrations close to 90 g/kg. This could be problematic as increased concentrations lead to precipitation and therefore localized fouling [48]. Furthermore, disposal of brine at greater concentrations increases the risk of pollution and could be subject to regulation depending on the location.

The final parameter of interest within the general hierarchy is the product salt concentration C_p . It is expected to have no salt concentration in MED as it employs a distillation process with demisters that

prevent entrained saline droplets from combining with the produced water vapor. However, salt ions can permeate the membrane in RO and result in a flow with non-negligible C_p . MED, as expected, results in negligible product concentrations independent of M_d or C_f . RO, on the other hand, presents product concentrations ranging from 0.05 g/kg up to 0.90 g/kg at feed concentrations of 2 g/kg and 50 g/kg, respectively.

The General Output analysis results also suggest it is important to consider what the product water will be used for after desalination. While MED consistently results in water with negligible salt content, the RO permeate product can have salt concentrations up to 0.90 g/kg at high C_f . As a reference point, the World Health Organization defines palatable concentration limits for human consumption as follows: 0.2–0.3 g/kg for chloride, 0.2 g/kg for sodium, and 0.6 g/kg for total dissolved solids [140]. If the product water is used as municipal water, it must go through a post-desalination process regardless of what desalination method is used, however, the MED process will consistently produce water with negligible salt content as opposed to RO which could involve additional desalination.

4.2.2. Family hierarchy

MED and RO correspond to the thermal and molecular transport desalination families, respectively, and therefore, their family parameters cannot be directly cross-compared. However, it is important to consider them independently to understand potential tradeoffs associated to each system.

Fig. 13 shows the relation between mean E_{des} across the studied M_d ranges and C_f . All curves are superimposed for each desalination method indicating that P_{des} and M_d are directly correlated with a 1:1 ratio. E_{des} is the main point for cross-comparison in other studies whose analysis is usually restricted to sea water salinity ranges between 35 and 42 g/kg. The results closely match the energy consumption found at these concentrations for both MED and RO [12,13,141]. Furthermore, the results lie within the generalized ranges of 73 kWh/m³ and 2-4 kWh/m³ for MED and RO, respectively, determined in a previously conducted life cycle assessment analysis [142]. The change in E_{des} is positively correlated to C_f for both technologies. This can be expected from the increase in boiling point elevation and osmotic pressure that result from increasing feed concentration in MED and RO, respectively. It is important to note that E_{des} in both methods has a similar gradient with respect to C_f at low concentrations; however, while energy intensity in RO remains linear with a constant gradient, the gradient for MED starts increasing after roughly 25 g/kg thus, deviating from a linear relation.

Overall, E_{des} remains between 51 and 13 times larger for MED than RO. This difference is attributed to the greater energy requirements

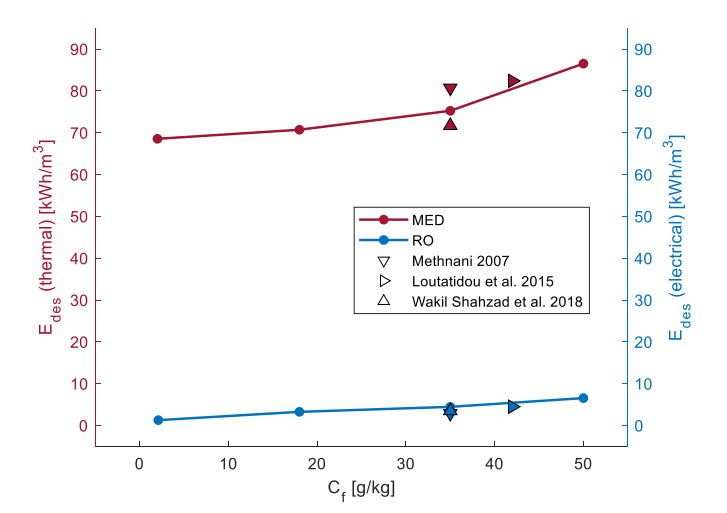


Fig. 13. Energy intensity (E_{des}) averaged across the studied M_d ranges in response to changes in feed water concentration.

involved in phase change which is inherent to the MED process. Despite the fact MED consistently shows a larger energy intensity, it must be noted that unlike RO, the process can run on low-grade energy. This could make the cost irrelevant if heat from a different process is available at a lower cost. For instance, in the MENA region, the average operating cost for RO can be about 4.6 times greater than MED, presumably due to low oil prices; however, the average total costs for both methods is relatively similar with differences of 0.04 ^3 [143]. The difference in the cost of energy is further extended for indirect solar desalination plants where the cost of water produced through RO can be up to about 13 times greater than MED even though the associated specific energy for desalination for RO can be between one and two orders of magnitude lower than that for MED [2]. RO presents a higher risk of fouling as it involves a permeation process, and therefore, preprocessing and maintenance can contribute to greater costs of desalination at higher feed salt concentrations and production rates. About 14% of the operating cost can be attributed to chemicals and post treatment [144] and pretreatment while structural and administrative tasks can add to 46% of the total cost [145]. The large discrepancies in energy consumption and total water cost further support the need of a methodological approach to benchmarking and cross-comparison as opposed to restricting the analysis to energy consumption alone.

Table 12 shows the remaining Family Hierarchy parameters for MED. It is evident that to achieve greater product flow rates, the system must generate more water vapor and therefore incur larger energy requirements with motive steam for evaporation independently of the value of C_f . Within a fixed M_d , there is a consistent positive correlation between M_p and C_f as increased salt concentration leads to a greater boiling point elevation and therefore larger energy requirements for evaporation.

The gain ratio (GR) for MED decreases as C_f becomes greater in all M_d ranges. From an energetic standpoint, the results show that the MED system becomes slightly less efficient as C_f increases, independent from M_d , since less product water can be produced by unit of motive steam used. There is about a 20% drop in GR between the lowest and highest C_f values.

Like GR, the specific cooling water (sM_{cw}), is independent of M_d and decreases with a total drop of about 40%. This highlights the fact that the MED is driven by evaporation and that the system must operate at higher temperatures because the boiling point is elevated with the presence of salt. The larger temperature differences between steam in the last effect and the intake cooling water improve heat transfer and reduce the requirements for cooling water. This would suggest that the MED process is optimized for larger salt concentrations, regardless of the required production.

The Family Hierarchy can give a notion of the performance of the

Table 12 Thermal family hierarchy results.

| | | MED | | |
|--------------|--------------|--------------|--------|-------------------------|
| M_d [kg/s] | C_f [g/kg] | M_p [kg/s] | GR [-] | sM _{cw} [g/kg] |
| 2.3 | 2 | 0.25 | 9.3 | 2.9 |
| | 18 | 0.25 | 9.0 | 2.8 |
| | 35 | 0.27 | 8.5 | 2.5 |
| | 50 | 0.31 | 7.5 | 1.7 |
| 70 | 2 | 7.5 | 9.3 | 2.9 |
| | 18 | 7.7 | 9.0 | 2.8 |
| | 35 | 8.2 | 8.5 | 2.5 |
| | 50 | 9.5 | 7.5 | 1.7 |
| 138 | 2 | 15 | 9.3 | 2.9 |
| | 18 | 15 | 9.0 | 2.8 |
| | 35 | 16 | 8.5 | 2.5 |
| | 50 | 19 | 7.5 | 1.7 |
| 1157 | 2 | 124 | 9.3 | 2.9 |
| | 18 | 128 | 9.1 | 2.8 |
| | 35 | 136 | 8.5 | 2.5 |
| | 50 | 156 | 7.5 | 1.7 |

desalination process and the tradeoffs associated with each method, but it cannot yield comparative conclusions as MED and RO come from different desalination families. The resulting GR from MED indicates that at the system produces about 9.3 times the mass flow rate of motive steam and reduces to about 7.3 with increasing C_f . This occurs due to the increasing energy required to overcome the higher intermolecular attraction between salt ions and water molecules resulting from higher feed salinities. Greater M_d flow requirements and higher C_f consistently result in greater motive steam demand. It is important to note that MED can work with low-grade steam and thus be combined with an existing process. Steam availability can constrain the production flow rates achieved through MED. An external steam generator can supply the full or partial steam load, but this results in additional operating costs. This Family parameter analysis highlights a tradeoff in MED where greater C_f results in lower GR, or increased steam demands per product water flow rate, but also results in a deceasing sM_{cw} and therefore less discharged cooling water. With respect to MED, this hierarchy yields valuable insight on the limitations imposed by energy availability and water supply and discharge.

4.2.3. Specific hierarchy

The Specific Hierarchy is redundant in this analysis since the studied systems are completely different, and therefore, the parameters cannot be cross compared. Nevertheless, a brief independent assessment of the resulting representative system size in response to changes in feed salinity can be important to consider. As shown in Table 13, the representative system size is expressed in the condenser area (A_c) in the case of MED and the total membra area (A_m) in the case of RO. In both desalination methods, the larger the production requirements require a larger system. Furthermore, for most cases the system size is also positively correlated to C_f . At 2 g/kg and with a product flow rate of 1157 kg/s, the membrane area for RO is larger and deviates from the trend. This occurs because the model considers such large flow rate as many parallel pressure vessels, therefore increasing one module in series, since adding a membrane module is equivalent to a discrete increase in system area, actually results in a larger total area than required for the desired M_d . It must be noted that the condenser area in MED is the effective area in the tube bundles of the heat exchanger while the system area in RO is the total surface area of the spiral-wound membrane modules. Generally, RO systems are more flexible in terms of size as membrane modules can be added to an existing system with relative ease as opposed to a condenser in MED which would require replacing the entire component.

4.3. Limitations

Although the presented simulations support the viability for

Table 13Relevant specific family hierarchy results.

| | | MED | RO |
|--------------|--------------|--------------------------------|-------------------------|
| M_d [kg/s] | C_f [g/kg] | $\overline{A_c \text{ [m}^2]}$ | A_m [m ²] |
| 2.3 | 2 | 37 | 53 |
| | 18 | 41 | 55 |
| | 35 | 49 | 96 |
| | 50 | 63 | 155 |
| 70 | 2 | 1138 | 1653 |
| | 18 | 1262 | 1694 |
| | 35 | 1481 | 2934 |
| | 50 | 1915 | 4684 |
| 138 | 2 | 2242 | 3218 |
| | 18 | 2486 | 3314 |
| | 35 | 2918 | 5779 |
| | 50 | 3772 | 9304 |
| 1157 | 2 | 18,821 | 128,411 |
| | 18 | 20,873 | 28,015 |
| | 35 | 24,499 | 48,353 |
| | 50 | 31,671 | 78,113 |

integrating different desalination methods into the proposed framework, the major limitation remains at the validity ranges for intake product flow rate (M_d) and intake salinity (C_f) of the representative models. Most of the constructed models, including TVC, MED, HDH, and RO, are validated within a 10% difference of their corresponding literature model and show excellent agreement with more than 24 independent publications in total. However, models such as EDS or CDI that rely on empirical correlations and coefficients that are valid only for the specific system and operating conditions have a much narrower operational range that does not completely intersect with the other models. Therefore, the proposed framework can only be deployed at these reduced ranges potentially showing incomplete results. Bench scale systems will need future modeling upgrades to represent electric energy consumption for a commercial system that could potentially include not only the electric energy for electrodes but also for circulation pumps. More appropriate general models for these desalination processes are a subject of ongoing research and updating the existing models can solve this limitation. The hierarchical parameter classification framework presented in this paper provides a clear structure to easily incorporate published models which can either expand the capabilities of the current metamodels or incorporate new models for novel desalination methods.

The present study focuses on specific energy consumption and the associated operational cost as a key parameter for cross-comparison. We suggest that the type of energy associated to MED and RO justifies the current market share panorama based on the costs of steam and electricity generation. It is possible that inadequate operation and maintenance are more expensive than energy itself in an actual facility. This is a view of energy which is an important piece of the puzzle, but there are many other aspects of desalination technologies which are out of the scope of this work. Additional studies, such as a full lifecycle analysis can provide insights into levelized cost calculations and therefore better conclusions about the financials associated to each desalination process.

5. Conclusions

This work aims to evaluate technologically possible operation conditions for different desalination technologies, which set targets to achieve or exceeds in the development of new desalination systems. This study developed reduced-order desalination metamodels and a framework to conduct a cross-comparative analysis by classifying input and output parameters according to an analytical hierarchy. The metamodels show excellent agreement with published data as the results have a maximum 9% error when compared to the results of models in the existing literature. The proposed framework compares the general outputs of (a) Thermovapor Compression (TVC), Multi-Effect Distillation (MED), Humidification-Dehumidification (HDH) in the thermal family of desalination methods, and (b) Reverse Osmosis (RO), Electrodialysis (EDS), and Capacitive Deionization (CDI) in the molecular transport family of desalination methods, at different operational condition ranges. The study provided a detailed comparative analysis between the most popular desalination technologies, MED and RO.

The first part of this study used the developed framework for a comparison between the studied desalination methods and their corresponding operational points from the most representative model in the literature. The results highlight the importance of system scalability in catering towards wider ranges of salt concentrations and production flow rates. The simulation results at the operational conditions presented in the literature for each representative model highlights the lack of overlap in product flow rate ranges that the models can simulate, which makes cross-comparison more challenging as some correlations cannot be used beyond the intended operational range. Indeed, there are instances where operation ranges are reported in the literature, but the number of undisclosed parameters makes their implementation difficult. Future research would be required to expand modeling capabilities of the presented metamodels by linking additional modeling correlations. Nevertheless, integrating the current metamodels into a single

simulation frame is appropriate as the existing models exhibit partial overlaps in feed water salt concentration and show similar sensitivity to feed salinity independent from product flow rate. Specifically, the operation points from the most representative literature models employ a salinity range of 1.6 to 2.4 g/kg for both Capacitive Deionization and Reverse Osmosis, a range of 28 to 42 g/kg for Thermovapor Compression and Humidification-Dehumidification desalination, and a range of 37 to 55 g/kg for Multi-Effect Distillation, and there is a common increase in energy intensity for each increase in feed salinity. The presented comparative analysis suggests this relationship is consistent for MED and RO when testing wider operation ranges.

From a modeling perspective, small scale, or newer desalination methods such as TVC, HDH, EDS, and CDI, do not yet offer the required system scalability reflected in ranges for which correlations hold valid, to compete with the established MED and RO processes. This is particularly evidenced in the humidifier calculations for HDH, the limiting current density in EDS, and the ion adsorption in CDI. All of these critical parameters are estimated with empirical relations that are specific to the system and operating conditions and are not generalizable to larger system scales and other operational regimes. MED and RO are constructed in a modular form for either evaporator effects or membrane units governed by less constrained equations that can be easily added to expand capacity and therefore cover the largest operational spaces. Until new developments within the other desalination processes allow such scalability, the commercial competitiveness of TVC, HDH, EDS and CDI would be limited to the specific conditions of low production flow rates and in the case of the molecular transport processes, low salt concentrations that are found in the literature. Further research is required within each desalination method to enable generalized predictive modeling to facilitate adoption and fair cross-comparison in the long term.

The second part of the study uses the simulation framework in a cross-comparative analysis between MED and RO, which are the most widely used desalination technologies in the current market. We find that recovery ratio can be expressed as an ideal operation line that can be used to assess how far from ideal operation a system is. These functions give targets for existing facility managers to understand if their technology is optimally designed or operated. The first concluding remark from this analysis points at the wide operational regimes in the conducted simulations. The operational space considered in product water flow rates ranges from bench to large scale production, and feed salinity levels concentrations range from irrigation to brine. The ability to cover such a large range of operational regimes is the first objective that experimental desalination technologies need to reach to become competitive in the marketplace. The conducted comparative analysis identified the tradeoffs, strengths, and weaknesses that each system has through a systematic review of General-, Family-, and System-level parameters. This can also be used to identify potential niche opportunities that experimental desalination methods could target. For all ranges, energy intensity is an order of magnitude larger for MED than RO. This difference results from the greater energy requirements involved in phase change in the MED process and can be equalized by the higher cost of electricity compared to low grade steam. Furthermore, at high feed salinities MED shows 50% greater brine production values than RO, whose discharged brine can have concentrations close to 90 g/kg, while MED restricts brine concentration at 72 g/kg. In addition, MED product concentration is consistently negligible as opposed to RO for which product concentration ranges from about 0.1 g/kg to 0.9 g/kg for feed concentrations of 2 g/kg and 50 g/kg, respectively. Therefore, although MED incurs a larger energy intensity, the lower energy costs and greater controllability of brine and product streams justify such a difference. For actual desalination plants, the thermodynamic differences between MED and RO result in similar utility costs due to the variation in the costs of thermal and electrical energy. Furthermore, besides energy availability and costs, other considerations in selecting the type of desalination plant involve available space for the plant, system lifetime, and local

regulations regarding brine disposal, including temperature, quantity, and salinity.

In conclusion, energy intensity alone or isolated model parameters are not appropriate for determining the viability of desalination processes. Instead, an inclusive approach relating model inputs and outputs across the same analytical hierarchy clearly outlines the energetic tradeoffs that a desalination system presents. Taking this into account, the best desalination method is the one that fulfills the operational requirements while recognizing energy availability and its costs. Practical constraints, such as the available space for the desalination facility and the disposal of the brine, also play a major role in establishing the most suitable desalination system. Overall, this study developed an analytical framework to desalination modeling because it allowed for systemic comparisons among all desalination methods.

CRediT authorship contribution statement

Sebastian A. Romo: Conceptualization, Methodology, Software, Validation, Formal analysis, Investigation, Data Curation, Writing – Original Draft, Writing – Review & Editing, Visualization. **Nicholas Mattise:** Conceptualization, Methodology, Software, Data Curation, Writing – Review & Editing. **Jelena Srebric:** Conceptualization, Resources, Writing – Review & Editing, Visualization, Supervision, Project administration, Funding acquisition.

Declaration of competing interest

The authors declare that they have no known competing financial interests or personal relationships that could have appeared to influence the work reported in this paper.

Acknowledgments

Funding: This work was supported by the U.S. Department of Energy Office of Energy Efficiency and Renewable Energy [DE-EE0008402].

The authors gratefully acknowledge Dr. Bahaman Abbasi (Oregon State University, USA) for the fruitful discussion during concept development phase of this study.

Appendix A. Supplementary data

Supplementary data to this article includes metamodel validation with literature model data and meta-study data. Metamodel source code available online at: https://desal.city.umd.edu. Supplementary data to this article can be found online at https://doi.org/10.1016/j.desal.20 21.115474.

References

- D. Brogioli, F.La Mantia, N.Y. Yip, Thermodynamic analysis and energy efficiency of thermal desalination processes, Desalination 428 (July 2017) (Feb. 2018) 29–39, https://doi.org/10.1016/j.desal.2017.11.010.
- [2] M.T. Ali, H.E.S. Fath, P.R. Armstrong, A comprehensive techno-economical review of indirect solar desalination, Renew. Sust. Energ. Rev. 15 (8) (Oct. 2011) 4187–4199, https://doi.org/10.1016/j.rser.2011.05.012.
- [3] K.V. Reddy, N. Ghaffour, Overview of the cost of desalinated water and costing methodologies, Desalination 205 (1-3) (Feb. 2007) 340–353, https://doi.org/ 10.1016/j.desal.2006.03.558.
- [4] S. Ahmadvand, B. Abbasi, B. Azarfar, M. Elhashimi, X. Zhang, B. Abbasi, Looking beyond energy efficiency: an applied review of water desalination technologies and an introduction to capillary-driven desalination, Water 11 (4) (Apr. 2019) 696. https://doi.org/10.3390/w11040696.
- [5] A. Al-Karaghouli, L.L. Kazmerski, Energy consumption and water production cost of conventional and renewable-energy-powered desalination processes, Renew. Sust. Energ. Rev. 24 (Aug. 2013) 343–356, https://doi.org/10.1016/j. rser.2012.12.064.
- [6] Y. Ghalavand, M.S. Hatamipour, A. Rahimi, A review on energy consumption of desalination processes, Desalin. Water Treat. 54 (6) (Mar. 2014) 1–16, https:// doi.org/10.1080/19443994.2014.892837.

- [7] Z. Wang, Y. Wang, G. Xu, J. Ren, Sustainable desalination process selection: decision support framework under hybrid information, Desalination 465 (January) (Sep. 2019) 44–57, https://doi.org/10.1016/j.desal.2019.04.022.
- [8] R. Semiat, Energy issues in desalination processes, Environ. Sci. Technol. 42 (22) (Nov. 2008) 8193–8201, https://doi.org/10.1021/es801330u.
- [9] T. Altmann, J. Robert, A. Bouma, J. Swaminathan, J.H. Lienhard, Primary energy and exergy of desalination technologies in a power-water cogeneration scheme, Appl. Energy 252 (January) (Oct. 2019) 113319, https://doi.org/10.1016/j. apenergy.2019.113319.
- [10] G.P. Thiel, E.W. Tow, L.D. Banchik, H.W. Chung, J.H. Lienhard, Energy consumption in desalinating produced water from shale oil and gas extraction, Desalination 366 (Jun. 2015) 94–112, https://doi.org/10.1016/j. desal.2014.12.038.
- [11] M. Qin, et al., Comparison of energy consumption in desalination by capacitive deionization and reverse osmosis, Desalination 455 (January) (2019) 100–114, https://doi.org/10.1016/j.desal.2019.01.003.
- [12] S. Loutatidou, H.A. Arafat, Techno-economic analysis of MED and RO desalination powered by low-enthalpy geothermal energy, Desalination 365 (2015) 277–292, https://doi.org/10.1016/j.desal.2015.03.010.
- [13] M. Methnani, Influence of fuel costs on seawater desalination options, Desalination 205 (1–3) (2007) 332–339, https://doi.org/10.1016/j. desal.2006.02.058.
- [14] N.C. Wright, A.G. Winter, Justification for community-scale photovoltaicpowered electrodialysis desalination systems for inland rural villages in India, Desalination 352 (2014) 82–91, https://doi.org/10.1016/j.desal.2014.07.035.
- [15] R. Zhao, S. Porada, P.M. Biesheuvel, A. van der Wal, Energy consumption in membrane capacitive deionization for different water recoveries and flow rates, and comparison with reverse osmosis, Desalination 330 (Dec. 2013) 35–41, https://doi.org/10.1016/j.desal.2013.08.017.
- [16] K. Mistry, J. Lienhard, Generalized least energy of separation for desalination and other chemical separation processes, Entropy 15 (12) (May 2013) 2046–2080, https://doi.org/10.3390/e15062046.
- [17] M.H. Sharqawy, J.H. Lienhard, S.M. Zubair, Thermophysical properties of seawater: a review of existing correlations and data, Desalin. Water Treat. 16 (1–3) (Apr. 2010) 354–380, https://doi.org/10.5004/dwt.2010.1079.
- [18] K.G. Nayar, M.H. Sharqawy, L.D. Banchik, J.H. Lienhard, Thermophysical properties of seawater: a review and new correlations that include pressure dependence, Desalination 390 (2016) 1–24, https://doi.org/10.1016/j. desal.2016.02.024.
- [19] I. Foxboro, in: "Conductivity Ordering Guide," Price Sheet. Invensys Foxboro, Foxboro, Massachusetts, 1999, pp. 1–2.
- [20] H. Ucok, I. Ershaghi, G.R. Olhoeft, Electrical resistivity of geothermal brines, J. Pet. Technol. 32 (04) (Apr. 1980) 717–727, https://doi.org/10.2118/7878-PA.
- [21] M. Holmgren, X Steam, Thermodynamic properties of water and steam [Online]. Available:, in: MATLAB Central File Exchange, 2007 https://www.mathworks.com/matlabcentral/fileexchange/9817-x-steam-thermodynamic-properties-of-water-and-steam.
- [22] H.T. El-Dessouky, H.M. Ettouney, Fundamentals of Salt Water Desalination, 1st ed., Elsevier Science Ltd. 2002.
- [23] A. Picard, R.S. Davis, M. Gläser, K. Fujii, Revised formula for the density of moist air (CIPM-2007), Metrologia 45 (2) (Apr. 2008) 149–155, https://doi.org/ 10.1088/0026-1394/45/2/004.
- [24] J.G. Ji, R.Z. Wang, L.X. Li, H. Ni, Simulation and analysis of a single-effect thermal vapor-compression desalination system at variable operation conditions, Chem. Eng. Technol. 30 (12) (2007) 1633–1641, https://doi.org/10.1002/ ceat.200700303.
- [25] M.A. Darwish, F. Al-Juwayhel, H.K. Abdulraheim, Multi-effect boiling systems from an energy viewpoint, Desalination 194 (1–3) (2006) 22–39, https://doi.org/ 10.1016/j.desal.2005.08.029.
- [26] H. Ettouney, Design and analysis of humidification dehumidification desalination process, Desalination 183 (1–3) (2005) 341–352, https://doi.org/10.1016/j. desal.2005.03.039.
- [27] J. Zhang, Computational Modeling and Evaluation of Reverse Osmosis, Stanford University, 2015.
- [28] H.J. Lee, F. Sarfert, H. Strathmann, S.H. Moon, Designing of an electrodialysis desalination plant, Desalination 142 (3) (2002) 267–286, https://doi.org/ 10.1016/S0011-9164(02)00208-4.
- [29] M. Qin, Comparison of energy consumption in desalination by capacitive deionization and reverse osmosis, Desalination 455 (November 2018) (2019) 100–114, https://doi.org/10.1016/j.desal.2019.01.003.
- [30] S.A. Romo, N.W. Mattise, J. Srebric, DESAL, in: City@UMD & The University of Maryland, College Park, 2021. https://desal.city.umd.edu/.
- [31] W. El-Mudir, Performance evaluation of a small size TVC desalination plant, Desalination 165 (2004) 269–279, https://doi.org/10.1016/j. desa1.2004.06.031.
- [32] N.M. Al-Najem, M.A. Darwish, F.A. Youssef, Thermovapor compression desalters: energy and availability — analysis of single- and multi-effect systems, Desalination 110 (3) (Sep. 1997) 223–238, https://doi.org/10.1016/S0011-9164 (97)00101-X.
- [33] S. Shen, S. Zhou, Y. Yang, L. Yang, X. Liu, Study of steam parameters on the performance of a TVC-MED desalination plant, Desalin. Water Treat. 33 (1–3) (Sep. 2011) 300–308, https://doi.org/10.5004/dwt.2011.2653.
- [34] S.M.A.N.R. Abadi, R. Kouhikamali, CFD-aided mathematical modeling of thermal vapor compressors in multiple effects distillation units, Appl. Math. Model. 40 (15–16) (2016) 6850–6868, https://doi.org/10.1016/j.apm.2016.02.032.

- [35] A.M. Bonanos, Physical modeling of thermo-compressor for desalination applications, Desalination 412 (2017) 13–19, https://doi.org/10.1016/j. desal.2017.03.004.
- [36] A.O.Bin Amer, Development and optimization of ME-TVC desalination system, Desalination 249 (3) (Dec. 2009) 1315–1331, https://doi.org/10.1016/j. desal.2009.06.026.
- [37] H. El-Dessouky, Modelling and simulation of the thermal vapour compression desalination process, in: Nuclear Desalination of Sea Water, 1997, pp. 315–338. https://inis.iaea.org/search/search.aspx?orig.q=RN:29023185.
- [38] R.R.B. Power, Steam Jet Ejectors for the Process Industries, Second Edi, McGraw-Hill Inc, New York, 1994.
- [39] A.S. Hassan, M.A. Darwish, Performance of thermal vapor compression, Desalination 335 (1) (2014) 41–46. http://www.scopus.com/inward/record.url? eid=2-s2.0-84891656599&partnerID=40&md5=f6bb7d386d150da22dbd809b 30c3ca5a
- [40] H. El-Dessouky, I. Alatiqi, S. Bingulac, H. Ettouney, Steady-state analysis of the multiple effect evaporation desalination process, Chem. Eng. Technol. 21 (5) (1998) 437–451, https://doi.org/10.1002/(SICI)1521-4125(199805)21:5<437:: AID-CEAT437>3.0.CO;2-D.
- [41] M.A. Darwish, Thermal analysis of vapor compression desalination system, Desalination 69 (3) (Jan. 1988) 275–295, https://doi.org/10.1016/0011-9164 (88)80030-4.
- [42] M.A. Sharaf, A.S. Nafey, L. García-Rodríguez, Thermo-economic analysis of solar thermal power cycles assisted MED-VC (multi effect distillation-vapor compression) desalination processes, Energy 36 (5) (2011) 2753–2764, https:// doi.org/10.1016/j.energy.2011.02.015.
- [43] F. Al-Juwayhel, H. El-Dessouky, H. Ettouney, Analysis of single-effect evaporator desalination systems combined with vapor compression heat pumps, Desalination 114 (3) (1997) 253–275, https://doi.org/10.1016/S0011-9164(98)00017-4.
- [44] H.T. El-Dessouky, I.M. Alatiqi, H.M. Ettouney, N.S. Al-Deffeeri, Performance of wire mesh mist eliminator, Chem. Eng. Process. Process Intensif. 39 (2) (2000) 129–139, https://doi.org/10.1016/S0255-2701(99)00033-1.
- [45] H. El-Dessouky, H. Ettouney, Single-effect thermal vapor-compression desalination process: thermal analysis, Heat Transf. Eng. 20 (2) (1999) 52–68, https://doi.org/10.1080/014576399271583.
- [46] K.H. Mistry, M.A. Antar, J.H. V Lienhard, An improved model for multiple effect distillation, Desalin. Water Treat. 51 (4–6) (Jan. 2013) 807–821, https://doi.org/ 10.1080/19443994.2012.703383.
- [47] M. Alahmad, Factors affecting scale formation in sea water environments an experimental approach, Chem. Eng. Technol. 31 (1) (Jan. 2008) 149–156, https://doi.org/10.1002/ceat.200700062.
- [48] M. Al-Ahmad, F.A. Aleem, Scale formation and fouling problems and their predicted reflection on the performance of desalination plants in Saudi Arabia, Desalination 96 (1–3) (Jun. 1994) 409–419, https://doi.org/10.1016/0011-9164 (94)85190.5
- [49] M.A. Darwish, H.K. Abdulrahim, Feed water arrangements in a multi-effect desalting system, Desalination 228 (1–3) (2008) 30–54, https://doi.org/10.1016/ i.desal.2007.05.039
- [50] P. Palenzuela, A.S. Hassan, G. Zaragoza, D.C. Alarcón-Padilla, Steady state model for multi-effect distillation case study: plataforma solar de Almería MED pilot plant, Desalination 337 (1) (2014) 31–42, https://doi.org/10.1016/j. desal.2013.12.029.
- [51] F.N. Alasfour, M.A. Darwish, A.O. Bin Amer, Thermal analysis of ME-TVC+MEE desalination systems, Desalination 174 (1) (2005) 39–61, https://doi.org/ 10.1016/j.desal.2004.08.039.
- [52] S. Casimiro, J. Cardoso, C. Ioakimidis, J. Farinha Mendes, C. Mineo, A. Cipollina, MED parallel system powered by concentrating solar power (CSP). Model and case study: Trapani, Sicily, Desalin. Water Treat. 55 (12) (2015) 3253–3266, https://doi.org/10.1080/19443994.2014.940222.
- [53] M. Shakouri, H. Ghadamian, R. Sheikholeslami, Optimal model for multi effect desalination system integrated with gas turbine, Desalination 260 (1–3) (2010) 254–263, https://doi.org/10.1016/j.desal.2010.03.032.
- [54] B. Ortega-Delgado, P. Palenzuela, D.C. Alarcón-Padilla, Parametric study of a multi-effect distillation plant with thermal vapor compression for its integration into a rankine cycle power block, Desalination 394 (2016) 18–29, https://doi. org/10.1016/j.desal.2016.04.020.
- [55] H.T. El-Dessouky, H.M. Ettouney, Multiple-effect evaporation desalination systems: thermal analysis, Desalination 125 (1–3) (1999) 259–276, https://doi. org/10.1016/S0011-9164(99)00147-2.
- [56] M. Ameri, S.S. Mohammadi, M. Hosseini, M. Seifi, Effect of design parameters on multi-effect desalinationsystem specifications, Desalination 245 (1–3) (Sep. 2009) 266–283, https://doi.org/10.1016/j.desal.2008.07.012.
- [57] A. Cipollina, G. Micale, L. Rizzuti, A critical assessment of desalination operations in Sicily, Desalination 182 (1–3) (2005) 1–12, https://doi.org/10.1016/j. desal.2005.03.004.
- [58] C. Temstet, G. Canton, J. Laborie, A. Durante, A large high-performance MED plant in Sicily, Desalination 105 (1–2) (1996) 109–114, https://doi.org/10.1016/ 0011-9164(96)00064-1.
- [59] D. Zhao, J. Xue, S. Li, H. Sun, Q. Dong Zhang, Theoretical analyses of thermal and economical aspects of multi-effect distillation desalination dealing with highsalinity wastewater, Desalination 273 (2–3) (2011) 292–298, https://doi.org/ 10.1016/j.desal.2011.01.048.
- [60] M.M. Ashour, Steady state analysis of the Tripoli west LT-HT-MED plant, Desalination 152 (1–3) (2003) 191–194, https://doi.org/10.1016/S0011-9164 (02)01062-7.

- [61] P. Sharan, S. Bandyopadhyay, Integration of thermo-vapor compressor with multiple-effect evaporator, Appl. Energy 184 (2016) 560–573, https://doi.org/ 10.1016/j.apenergy.2016.10.037.
- [62] V. Dvornikov, Seawater multi-effect distillation energized by a combustion turbine, Desalination 127 (3) (2000) 261–269, https://doi.org/10.1016/S0011-9164(00)00015-1.
- [63] M.A. Sharaf, A.S. Nafey, L. García-Rodríguez, Exergy and thermo-economic analyses of a combined solar organic cycle with multi effect distillation (MED) desalination process, Desalination 272 (1–3) (2011) 135–147, https://doi.org/ 10.1016/j.desal.2011.01.006.
- [64] M.A. Darwish, F.Al Juwayhel, H. Kamal, Multi-effect boiling system meb: an energy viewpoint, in: Sustainable Development of Energy, Water and Environment Systems vol. 194, Jun. 2007, pp. 351–372, https://doi.org/ 10.1142/9789812771285_0032, no. 1–3.
- [65] M.A. Sharaf, Design and Simulation of Solar Desalination Systems, Suez Canal University, 2011.
- [66] M.H. Sharqawy, M.A. Antar, S.M. Zubair, A.M. Elbashir, Optimum thermal design of humidification dehumidification desalination systems, Desalination 349 (2014) 10–21, https://doi.org/10.1016/j.desal.2014.06.016.
- [67] M. Khedr, Techno-economic investigation of an air humidification-dehumidification desalination process, Chem. Eng. Technol. 16 (4) (Aug. 1993) 270–274, https://doi.org/10.1002/ceat.270160410.
- [68] G. Al-Enezi, H. Ettouney, N. Fawzy, Low temperature humidification dehumidification desalination process, Energy Convers. Manag. 47 (4) (Mar. 2006) 470–484, https://doi.org/10.1016/j.enconman.2005.04.010.
- [69] G.P. Narayan, M.H. Sharqawy, J.H. V Lienhard, S.M. Zubair, Thermodynamic analysis of humidification dehumidification desalination cycles, Desalin. Water Treat. 16 (1–3) (2010) 339–353, https://doi.org/10.5004/dwt.2010.1078.
- [70] S. Farsad, A. Behzadmehr, Analysis of a solar desalination unit with humidification-dehumidification cycle using DoE method, Desalination 278 (1–3) (2011) 70–76, https://doi.org/10.1016/j.desal.2011.05.008.
- [71] S. Dehghani, A. Date, A. Akbarzadeh, An experimental study of brine recirculation in humidification-dehumidification desalination of seawater, Case Stud. Therm. Eng. 14 (December) (2018) 2019, https://doi.org/10.1016/j. csite.2019.100463.
- [72] M. Al-Sahali, H.M. Ettouney, Humidification dehumidification desalination process: design and performance evaluation, Chem. Eng. J. 143 (1–3) (2008) 257–264, https://doi.org/10.1016/j.cej.2008.04.030.
- [73] S.M. Zubair, M.A. Antar, S.M. Elmutasim, D.U. Lawal, Performance evaluation of humidification-dehumidification (HDH) desalination systems with and without heat recovery options: an experimental and theoretical investigation, Desalination 436 (October 2017) (2018) 161–175, https://doi.org/10.1016/j. desal.2018.02.018.
- [74] P.T. Tsilingiris, Thermophysical and transport properties of humid air at temperature range between 0 and 100 °C, Energy Convers. Manag. 49 (5) (2008) 1098–1110, https://doi.org/10.1016/j.encomman.2007.09.015.
- [75] SFitz, AirProperties [Online]. Available:, in: GitHube, 2021 https://github.com/s ifitz/AirProperties.
- [76] M.M. Farid, S. Parekh, J.R. Selman, S. Al-Hallaj, Solar desalination with a humidification-dehumidification cycle: mathematical modeling of the unit, Desalination 151 (2) (2003) 153–164, https://doi.org/10.1016/S0011-9164(02) 00994-3.
- [77] S. Farsad, A. Behzadmehr, S.M.H. Sarvari, Numerical analysis of solar desalination using humidification—dehumidification cycle, Desalin. Water Treat. 19 (1–3) (2010) 294–300, https://doi.org/10.5004/dwt.2010.1487.
- [78] M.H. Hamed, A.E. Kabeel, Z.M. Omara, S.W. Sharshir, Mathematical and experimental investigation of a solar humidification-dehumidification desalination unit, Desalination 358 (2015) 9–17, https://doi.org/10.1016/j. desal.2014.12.005.
- [79] G. Franchini, A. Perdichizzi, Modeling of a solar driven HD (humidification-dehumidification) desalination system, Energy Procedia 45 (2014) 588–597, https://doi.org/10.1016/j.egypro.2014.01.063.
- [80] E.H. Amer, H. Kotb, G.H. Mostafa, A.R. El-Ghalban, Theoretical and experimental investigation of humidification-dehumidification desalination unit, Desalination 249 (3) (2009) 949–959. https://doi.org/10.1016/j.desal.2009.06.063
- 249 (3) (2009) 949–959, https://doi.org/10.1016/j.desal.2009.06.063.
 [81] R. Santosh, G. Kumaresan, S. Selvaraj, T. Arunkumar, R. Velraj, Investigation of humidification-dehumidification desalination system through waste heat recovery from household air conditioning unit, Desalination 467 (May) (2019) 1–11, https://doi.org/10.1016/j.desal.2019.05.016.
- [82] K.G. Tay, L. Song, A more effective method for fouling characterization in a full-scale reverse osmosis process, Desalination 177 (1–3) (Jun. 2005) 95–107, https://doi.org/10.1016/j.desal.2004.11.017.
- [83] S.A. Avlonitis, M. Pappas, K. Moutesidis, A unified model for the detailed investigation of membrane modules and RO plants performance, Desalination 203 (1-3) (2007) 218–228, https://doi.org/10.1016/j.desal.2006.04.009.
- [84] H.J. Oh, T.M. Hwang, S. Lee, A simplified simulation model of RO systems for seawater desalination, Desalination 238 (1–3) (2009) 128–139, https://doi.org/ 10.1016/j.desal.2008.01.043.
- [85] V. Geraldes, N.E. Pereira, M.N. De Pinho, Simulation and optimization of medium-sized seawater reverse osmosis processes with spiral-wound modules, Ind. Eng. Chem. Res. 44 (6) (2005) 1897–1905, https://doi.org/10.1021/ ie049357s.
- [86] M. Khraisheh, et al., Osmotic pressure estimation using the pitzer equation for forward osmosis modelling, Environ. Technol. 41 (19) (Aug. 2020) 2533–2545, https://doi.org/10.1080/09593330.2019.1575476.

- [87] T. Kaghazchi, M. Mehri, M.T. Ravanchi, A. Kargari, A mathematical modeling of two industrial seawater desalination plants in the Persian Gulf region, Desalination 252 (1–3) (2010) 135–142, https://doi.org/10.1016/j. desal.2009.10.12
- [88] K.G. Nayar, Feasibility study of an electrodialysis system for in-home water desalination in urban India, Dev. Eng. 2 (December 2016) (2016) 38–46, https://doi.org/10.1016/j.deveng.2016.12.001.
- [89] M. Qasim, M. Badrelzaman, N.N. Darwish, N.A. Darwish, N. Hilal, Reverse osmosis desalination: a state-of-the-art review, Desalination 459 (December 2018) (Jun. 2019) 59–104, https://doi.org/10.1016/j.desal.2019.02.008.
- [90] E.-S. Jang, Influence of concentration polarization and thermodynamic nonideality on salt transport in reverse osmosis membranes, J. Membr. Sci. 572 (October 2018) (Feb. 2019) 668–675, https://doi.org/10.1016/j. memsri 2018 11 006
- [91] A.O. Sharif, et al., A new theoretical approach to estimate the specific energy consumption of reverse osmosis and other pressure-driven liquid-phase membrane processes, Desalin. Water Treat. 3 (1–3) (2009) 111–119, https://doi. org/10.5004/dwt.2009.295.
- [92] A. Altaee, Computational model for estimating reverse osmosis system design and performance: part-one binary feed solution, Desalination 291 (2012) 101–105, https://doi.org/10.1016/j.desal.2012.01.028.
- [93] X. Jin, A. Jawor, S. Kim, E.M.V. Hoek, Effects of feed water temperature on separation performance and organic fouling of brackish water RO membranes, Desalination 239 (1–3) (2009) 346–359, https://doi.org/10.1016/j. desal.2008.03.026.
- [94] J.C. Crittenden, R.R. Trussell, D.W. Hand, K.J. Howe, G. Tchobanoglous, Reverse osmosis, in: MWH's Water Treatment - Principles and Design, 3rd ed., John Wiley & Sons, 2012, pp. 1335–1414.
- [95] R.S. El-Emam, I. Dincer, Thermodynamic and thermoeconomic analyses of seawater reverse osmosis desalination plant with energy recovery, Energy 64 (Jan. 2014) 154–163, https://doi.org/10.1016/j.energy.2013.11.037.
- [96] N.M. Mazlan, D. Peshev, A.G. Livingston, Energy consumption for desalination a comparison of forward osmosis with reverse osmosis, and the potential for perfect membranes, Desalination 377 (Jan. 2016) 138–151, https://doi.org/ 10.1016/j.desal.2015.08.011.
- [97] A. Joseph, V. Damodaran, Dynamic simulation of the reverse osmosis process for seawater using LabVIEW and an analysis of the process performance, Comput. Chem. Eng. 121 (2019) 294–305, https://doi.org/10.1016/j. compchemeng.2018.11.001.
- [98] V. Haluch, E.F. Zanoelo, C.J.L. Hermes, Experimental evaluation and semiempirical modeling of a small-capacity reverse osmosis desalination unit, Chem. Eng. Res. Des. 122 (Jun. 2017) 243–253, https://doi.org/10.1016/j. cherd.2017.04.006.
- [99] D.E. Wiley, D.F. Fletcher, Techniques for computational fluid dynamics modelling of flow in membrane channels, J. Memb. Sci. 211 (1) (2003) 127–137, https:// doi.org/10.1016/S0376-7388(02)00412-X.
- [100] M. Ben Boudinar, W.T. Hanbury, S. Avlonitis, Numerical simulation and optimisation of spiral-wound modules, Desalination 86 (3) (1992) 273–290, https://doi.org/10.1016/0011-9164(92)80038-B.
- [101] G. Schock, A. Miquel, Mass transfer and pressure loss in spiral wound modules, Desalination 64 (Jan. 1987) 339–352, https://doi.org/10.1016/0011-9164(87) 90107-X
- [102] B.J. Mariñas, R.I. Urama, Modeling concentration-polarization in reverse osmosis spiral-wound elements, J. Environ. Eng. 122 (4) (Apr. 1996) 292–298, https://doi.org/10.1061/(ASCE)0733-9372(1996)122:4(292).
- [103] M. Shakaib, S.M.F. Hasani, M. Mahmood, CFD modeling for flow and mass transfer in spacer-obstructed membrane feed channels, J. Memb. Sci. 326 (2) (Jan. 2009) 270–284, https://doi.org/10.1016/j.memsci.2008.09.052.
- [104] F. Valero, A. Barcelo, R. Arbos, Electrodialysis technology theory and applications, no. 3, in: M. Schorr (Ed.), Desalination, Trends and Technologies vol. 189, InTech, 2011, pp. 1521–1535.
- [105] T. Mohammadi, A. Moheb, M. Sadrzadeh, A. Razmi, Modeling of metal ion removal from wastewater by electrodialysis, Sep. Purif. Technol. 41 (1) (2005) 73–82, https://doi.org/10.1016/j.seppur.2004.04.007.
- [106] J.M. Ortiz, et al., Brackish water desalination by electrodialysis: batch recirculation operation modeling, J. Membr. Sci. 252 (1–2) (2005) 65–75, https://doi.org/10.1016/j.memsci.2004.11.021.
- [107] M. Sadrzadeh, A. Kaviani, T. Mohammadi, Mathematical modeling of desalination by electrodialysis, Desalination 206 (1–3) (2007) 538–546, https:// doi.org/10.1016/j.desal.2006.04.062.
- [108] L. Karimi, A. Ghassemi, An empirical/theoretical model with dimensionless numbers to predict the performance of electrodialysis systems on the basis of operating conditions, Water Res. 98 (2016) 270–279, https://doi.org/10.1016/j. watres.2016.04.014.
- [109] M. La Cerva, et al., Determination of limiting current density and current efficiency in electrodialysis units, Desalination 445 (July) (2018) 138–148, https://doi.org/10.1016/j.desal.2018.07.028.
- [110] A. Campione, L. Gurreri, M. Ciofalo, G. Micale, A. Tamburini, A. Cipollina, Electrodialysis for water desalination: a critical assessment of recent developments on process fundamentals, models and applications, Desalination 434 (October 2017) (2018) 121–160, https://doi.org/10.1016/j. desal.2017.12.044.
- [111] M.Ben Sik Ali, A. Mnif, B. Hamrouni, Modelling of the limiting current density of an electrodialysis process by response surface methodology, Ionics (Kiel) 24 (2) (2018) 617–628, https://doi.org/10.1007/s11581-017-2214-7.

- [112] V. Geraldes, M.D. Afonso, Limiting current density in the electrodialysis of multiionic solutions, J. Membr. Sci. 360 (1–2) (2010) 499–508, https://doi.org/ 10.1016/j.memsci.2010.05.054.
- [113] R. Valerdi-Pérez, J. Ibáñez-Mengual, Current—voltage curves for an electrodialysis reversal pilot plant: determination of limiting currents, Desalination 141 (1) (Dec. 2001) 23–37, https://doi.org/10.1016/S0011-9164 (01)00386-1.
- [114] Y. Tanaka, Limiting current density of an ion-exchange membrane and of an electrodialyzer, J. Membr. Sci. 266 (1–2) (2005) 6–17, https://doi.org/10.1016/j. memsci.2005.05.005.
- [115] H.J. Lee, H. Strathmann, S.H. Moon, Determination of the limiting current density in electrodialysis desalination as an empirical function of linear velocity, Desalination 190 (1–3) (2006) 43–50, https://doi.org/10.1016/j. desal.2005.08.004.
- [116] A. Nakayama, Y. Sano, X. Bai, K. Tado, A boundary layer analysis for determination of the limiting current density in an electrodialysis desalination, Desalination 404 (2017) 41–49, https://doi.org/10.1016/j.desal.2016.10.013.
- [117] K.M. Chehayeb, D.M. Farhat, K.G. Nayar, J.H. Lienhard, Optimal design and operation of electrodialysis for brackish-water desalination and for high-salinity brine concentration, Desalination 420 (March) (Oct. 2017) 167–182, https://doi. org/10.1016/j.desal.2017.07.003.
- [118] Y. Gong, X.L. Wang, L.X. Yu, Process simulation of desalination by electrodialysis of an aqueous solution containing a neutral solute, Desalination 172 (2) (2005) 157–172, https://doi.org/10.1016/j.desal.2004.06.200.
- [119] N.C. Wright, S.R. Shah, S.E. Amrose, A.G. Winter, A robust model of brackish water electrodialysis desalination with experimental comparison at different size scales, Desalination 443 (April) (2018) 27–43, https://doi.org/10.1016/j. desal.2018.04.018.
- [120] Y. Tanaka, A computer simulation of feed and bleed ion exchange membrane electrodialysis for desalination of saline water, Desalination 254 (1–3) (May 2010) 99–107, https://doi.org/10.1016/j.desal.2009.12.008.
- [121] Y. Oren, Capacitive deionization (CDI) for desalination and water treatment past, present and future (a review), Desalination 228 (1–3) (2008) 10–29, https://doi.org/10.1016/j.desal.2007.08.005.
- [122] M.E. Suss, S. Porada, X. Sun, P.M. Biesheuvel, J. Yoon, V. Presser, Water desalination via capacitive deionization: what is it and what can we expect from it? Energy Environ. Sci. 8 (8) (2015) 2296–2319, https://doi.org/10.1039/ c5ec00519a
- [123] J.E. Dykstra, J. Dijkstra, A. van der Wal, H.V.M. Hamelers, S. Porada, On-line method to study dynamics of ion adsorption from mixtures of salts in capacitive deionization, Desalination 390 (Jul. 2016) 47–52, https://doi.org/10.1016/j. desal.2016.04.001.
- [124] J. Oladunni, J.H. Zain, A. Hai, F. Banat, G. Bharath, E. Alhseinat, A comprehensive review on recently developed carbon based nanocomposites for capacitive deionization: from theory to practice, Sep. Purif. Technol. 207 (March) (2018) 291–320, https://doi.org/10.1016/j.seppur.2018.06.046.
- [125] M. Qin, Corrigendum to 'Comparison of energy consumption in desalination by capacitive deionization and reverse osmosis' [DES 455 (2019) 100–114], Desalination 461 (April) (Jul. 2019) 55, https://doi.org/10.1016/j. desal 2019 03 016
- [126] M. Qin, et al., Response to comments on 'comparison of energy consumption in desalination by capacitive deionization and reverse osmosis', Desalination 462 (April) (Jul. 2019) 48–55, https://doi.org/10.1016/j.desal.2019.04.004.
- [127] M.E. Suss, et al., Capacitive desalination with flow-through electrodes, Energy Environ. Sci. 5 (11) (2012) 9511–9519, https://doi.org/10.1039/c2ee21498a.
- [128] E.N. Guyes, A.N. Shocron, A. Simanovski, P.M. Biesheuvel, M.E. Suss, A onedimensional model for water desalination by flow-through electrode capacitive

- deionization, Desalination 415 (2017) 8–13, https://doi.org/10.1016/j.desal.2017.03.013.
- [129] A. Rommerskirchen, B. Ohs, K.A. Hepp, R. Femmer, M. Wessling, Modeling continuous flow-electrode capacitive deionization processes with ion-exchange membranes, J. Membr. Sci. 546 (October 2017) (2018) 188–196, https://doi.org/ 10.1016/j.memsci.2017.10.026.
- [130] M.W. Saleem, W.S. Kim, Parameter-based performance evaluation and optimization of a capacitive deionization desalination process, Desalination 437 (February) (2018) 133–143, https://doi.org/10.1016/j.desal.2018.02.023.
- [131] J.E. Dykstra, R. Zhao, P.M. Biesheuvel, A. Van der Wal, Resistance identification and rational process design in capacitive deionization, Water Res. 88 (2016) 358–370, https://doi.org/10.1016/j.watres.2015.10.006.
- [132] R. Zhao, P.M. Biesheuvel, A. Van Der Wal, Energy consumption and constant current operation in membrane capacitive deionization, Energy Environ. Sci. 5 (11) (2012) 9520–9527, https://doi.org/10.1039/c2ee21737f.
- [133] C.A.R. Perez, O.N. Demirer, R.L. Clifton, R.M. Naylor, C.H. Hidrovo, Macro analysis of the electro-adsorption process in low concentration NaCl solutions for water desalination applications, J. Electrochem. Soc. 160 (3) (Jan. 2013) E13–E21, https://doi.org/10.1149/2.025303jes.
- [134] J.E. Dykstra, J. Dijkstra, A. Van der Wal, H.V.M. Hamelers, S. Porada, SUPPLEMENT on-line method to study dynamics of ion adsorption from mixtures of salts in capacitive deionization, Desalination 390 (2016) 47–52, https://doi. org/10.1016/j.desal.2016.04.001.
- [135] J.E. Dykstra, S. Porada, A. van der Wal, P.M. Biesheuvel, Supplementary information energy consumption in capacitive deionization – constant current versus constant voltage operation, Water Res. 143 (2018) 367–375, https://doi. org/10.1016/j.watres.2018.06.034.
- [136] L. Wang, S. Lin, Theoretical framework for designing a desalination plant based on membrane capacitive deionization, Water Res. 158 (2019) 359–369, https:// doi.org/10.1016/j.watres.2019.03.076.
- [137] S. Lin, Seawater desalination technology and engineering in China: a review, Desalination 498 (October 2020) (2021) 114728, https://doi.org/10.1016/j. desal.2020.114728.
- [138] H.T. El-Dessouky, H.M. Ettouney, F. Mandani, Performance of parallel feed multiple effect evaporation system for seawater desalination, Appl. Therm. Eng. 20 (17) (Dec. 2000) 1679–1706, https://doi.org/10.1016/S1359-4311(99) 00098-8
- [139] D. Hasson, A. Drak, R. Semiat, Inception of CaSO4 scaling on RO membranes at various water recovery levels, Desalination 139 (1–3) (Sep. 2001) 73–81, https:// doi.org/10.1016/S0011-9164(01)00296-X.
- [140] W. H. Organization, Guidelines for Drinking-water Quality: Fourth Edition Incorporating the First Addendum, Fourth Edi, 2017. Geneva.
- [141] M.Wakil Shahzad, M. Burhan, H.Soo Son, S.Jin Oh, K.Choon Ng, Desalination processes evaluation at common platform: a universal performance ratio (UPR) method, Appl. Therm. Eng. 134 (October 2017) (Apr. 2018) 62–67, https://doi.org/10.1016/j.applthermaleng.2018.01.098.
- [142] G. Raluy, L. Serra, J. Uche, Life cycle assessment of MSF, MED and RO desalination technologies, Energy 31 (13) (2006) 2361–2372, https://doi.org/ 10.1016/j.energy.2006.02.005.
- [143] J. Eke, A. Yusuf, A. Giwa, A. Sodiq, The global status of desalination: an assessment of current desalination technologies, plants and capacity, Desalination 495 (March) (Dec. 2020) 114633, https://doi.org/10.1016/j.desal.2020.114633.
- [144] Y. Dreizin, Ashkelon seawater desalination project off-taker's self costs, supplied water costs, total costs and benefits, Desalination 190 (1–3) (2006) 104–116, https://doi.org/10.1016/j.desal.2005.08.006.
- [145] R.Valladares Linares, Life cycle cost of a hybrid forward osmosis low pressure reverse osmosis system for seawater desalination and wastewater recovery, Water Res. 88 (7) (Jan. 2016) 225–234, https://doi.org/10.1016/j.watres.2015.10.017.